Neuroscience

Biophysical network modeling of temporal and stereotyped sequence propagation of neural activity in the premotor nucleus HVC

Reviewed Preprint
v1 • February 26, 2025
Not revised

Zeina Bou Diab, Marc Chammas, Arij Daou

Biomedical Engineering Program, American University of Beirut, Beirut, Lebanon

eLife Assessment

Birdsong production depends on precise neural sequences in a vocal motor nucleus HVC. In this **useful** biophysical model, Daou and colleagues identify specific biophysical parameters that result in sparse neural sequences observed in vivo. While the model is presently **incomplete** because it is overfit to produce sequences and therefore not robust to real biological variation, the model has the potential to address some outstanding issues in HVC function.

https://doi.org/10.7554/eLife.105526.1.sa2

Abstract

Stereotyped neural sequences are often exhibited in the brain, yet the neurophysiological mechanisms underlying their generation are not fully understood. Birdsong is a prominent model to study such behavior particularly because juvenile songbirds progressively learn from their tutors and by adulthood are able to sing stereotyped song patterns. The songbird premotor nucleus HVC coordinate motor and auditory activity responsible for learned vocalizations. The HVC comprises three neural populations that has distinct *in vitro* and *in vivo* electrophysiological responses. Typically, models that explain HVC's network either rely on intrinsic HVC circuitry to propagate sequential activity, rely on extrinsic feedback to advance the sequence or rely on both. Here, we developed a physiologically realistic neural network model incorporating the three classes of HVC neurons based on the ion channels and the synaptic currents that had been pharmacologically identified. Our model is based on a feedforward chain of microcircuits that encode for the different sub-syllabic segments (SSSs) and that interact with each other through structured feedback inhibition. The network reproduced the *in vivo* activity patterns of each class of HVC neurons, and unveiled key intrinsic and synaptic mechanisms that govern the sequential propagation of neural activity by highlighting important roles for the T-type Ca^{2+} current, Ca^{2+}-dependent K^{+} current, A-type K^{+} current, hyperpolarization activated inward current, as well as excitatory and inhibitory synaptic currents. The result is a biophysically realistic model that suggests an improved characterization of the HVC network responsible for song production in the songbird.

Introduction

Learned temporal sequences are expressed in many brain regions and play a critical role in temporal information encoding, such as navigation (Skaggs et al., 1996), the timing of motor actions (Wang et al., 2018), time generation (MacDonald et al., 2011; Pastalkova et al., 2008), decision making (Harvey et al., 2012; Schmitt et al., 2017) and skilled movement (Peters et al., 2014). Zebra finches sing remarkably stereotyped songs rendering them as an excellent model for studying the mechanisms underlying neural sequences (Hahnloser et al., 2002). The anatomical basis for song production and learning is a highly developed neural network known as the song system (**Fig. 1A**), with nucleus HVC exhibiting a rhythmic pattern-generating role encoding for the syllable order and the overall temporal structure of the birdsong (Fee & Goldberg, 2011; Fee et al., 2004; Fee & Scharff, 2010; Mooney, 2009; Yu & Margoliash, 1996).

There are three main neuronal populations in the HVC exhibiting different functional, cellular and pharmacological properties (Daou et al., 2013; Kubota & Taniguchi, 1998; Mooney, 2000; Mooney & Prather, 2005): neurons that project to the robust nucleus of arcopallium (RA; HVC_{RA}), neurons that project to Area X (HVC_X), and interneurons (HVCINT, **Fig. 1B**). HVCAv neurons (projecting to nucleus Avalanche) exists and play a role in song learning, yet their intrinsic and synaptic properties remains unknown (Roberts et al., 2017). Intracellular recordings showed that HVCRA, HVCX, and HVCINT neurons have distinctive *in vivo* and *in vitro* electrophysiological properties (Daou et al., 2013; Dutar et al., 1998; Kubota & Taniguchi, 1998; Mooney et al., 2001; Shea et al., 2010), which are orchestrated via a family of ion channels (Daou et al., 2013).

During singing, HVCRA neurons produce a single burst of spikes (~10 ms) that are tightly locked to the song (**Fig. 1C**, (Hahnloser et al., 2002; Kozhevnikov & Fee, 2007). HVCX neurons in their turn elicit 1-4 bursts that are also time-locked to vocalizations (**Fig. 1D**, (Kozhevnikov & Fee, 2007), while HVCINT neurons exhibit tonic activation (**Fig. 1C**), with bursting and suppression at different locations throughout the song (Amador et al., 2013; Cannon et al., 2015; Hahnloser et al., 2002; Kosche et al., 2015; Kozhevnikov & Fee, 2007; Long et al., 2010; Markowitz et al., 2015).

Several models of how sequence is generated within HVC have been proposed (Cannon et al., 2015; Drew & Abbott, 2003; Egger et al., 2020; Elmaleh et al., 2021; Galvis et al., 2018; Gibb et al., 2009a, 2009b; Hamaguchi et al., 2016; Jin, 2009; Long & Fee, 2008; Markowitz et al., 2015). These models either rely on intrinsic HVC circuitry to propagate sequential activity, rely on extrinsic feedback to advance the sequence or rely on both. The proposed models do not capture the complex details of spike morphology, do not include the right ionic currents, do not incorporate all classes of HVC neurons, or do not generate realistic firing patterns as seen *in vivo*.

Here, we developed a physiologically realistic network model incorporating the three classes of HVC neurons based on the ion channels and the synaptic currents that had been pharmacologically identified (Daou et al., 2013; Kosche et al., 2015; Mooney & Prather, 2005). Our model is based on a feedforward chain of microcircuits that encode for the different sub-syllabic segments (SSSs) and that interact with each other through structured feedback inhibition. The network developed unveiled key intrinsic and synaptic mechanisms that govern the sequential propagation of neural activity by highlighting important roles for the T-type Ca^{2+} current, Ca^{2+}-dependent K^+ current, A-type K^+ current, hyperpolarization activated inward current, as well as excitatory and inhibitory synaptic currents. Our model provides a new way of thinking about sequence generation during birdsong vocalizations and in network architectures more generally.

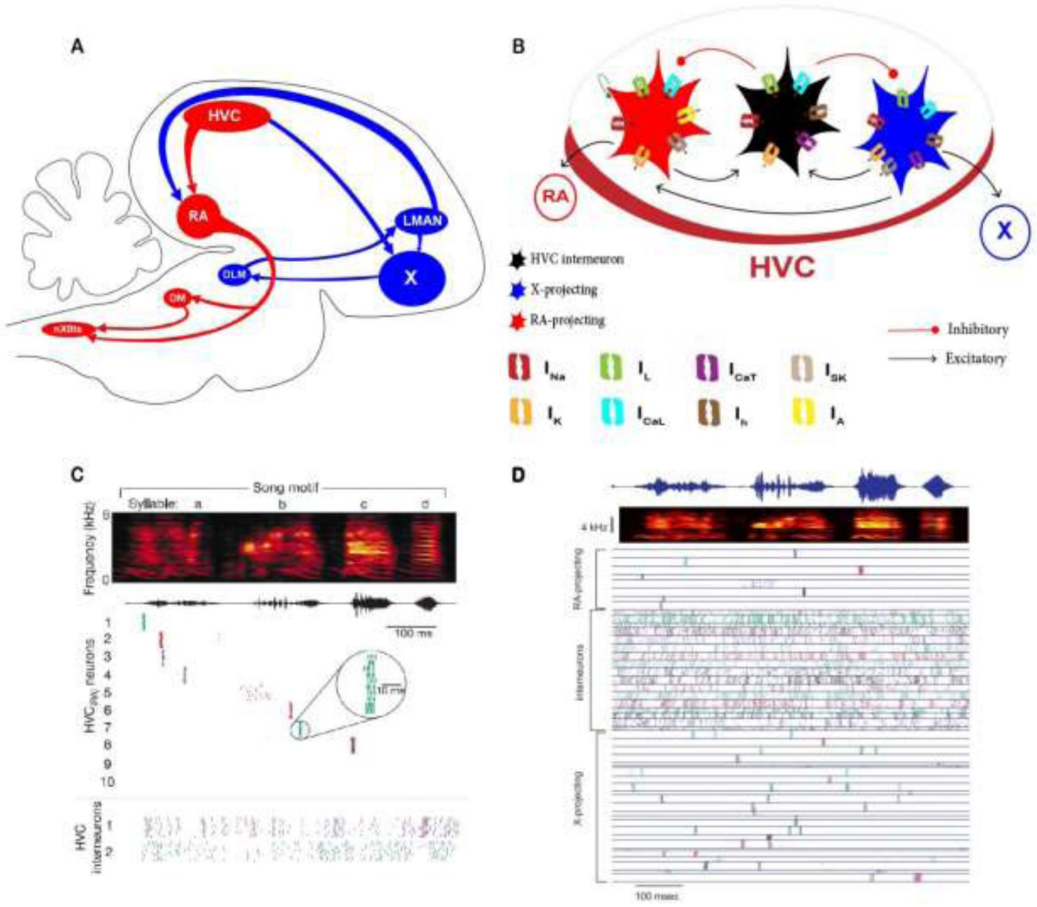

Figure 1.

Song system overview and general intrinsic and network properties of HVC neurons in vivo and in vitro.

A. Schematic diagram showing a sagittal view of the male zebra finch song system. The vocal motor pathway (VMP, red color) contains circuits that directly pattern song output. The anterior forebrain loop (AFP, blue color) pathway contains circuits that are important for song learning and plasticity. **B**. HVC includes multiple classes of neurons; HVC_X neurons that project to area X (blue), HVCRA neurons that project to nucleus RA (red) and HVC interneurons (HVC_{INT}, black). HVC_X and HVC_{RA} excite HVC_{INT} via AMPA and NMDA synapses (green arrow), while HVC_{INT} neurons inhibit both classes of projecting neurons via GABA synapses (brown arrows with circle heads). Each class of HVC neurons is characterized with its own family of ionic currents (Daou et al., 2013). **C**. HVC_{RA} neurons exhibit a very sparse activity during singing eliciting a single 4-6 ms burst at a single and exact moment in time during each rendition of the song. On the contrary, HVC interneurons burst densely throughout the song (Adopted from (Hahnloser et al., 2002)). **D**. Similar to HVC_{RA}, HVC_X neurons generate 1-4 bursts that are time-locked and highly stereotyped from one rendition of the song to another (Adopted from (Kozhevnikov & Fee, 2007)).

Methods

Single-compartment conductance-based Hodgkin-Huxley-type (HH) biophysical models of cells from the HVC were developed and connected together via biologically realistic synaptic currents. Simulations of these model neurons and of the model network composed of synaptically coupled HVC_{RA}, HVC_X, and HVC_{INT} neurons were performed using the ode45 numerical integrator in MATLAB (MathWorks). Source codes for each network will be made available online at our lab's website as well as on ModelDB. HVC model cells that are used to connect the networks exhibited ionic and synaptic currents that had been shown to be expressed pharmacologically (Daou et al., 2013; Kosche et al., 2015; Long et al., 2010; Mooney & Prather, 2005). The functional forms of activation/inactivation functions and time constants were based on previous published mathematical neural models (Daou et al., 2013; Destexhe & Babloyantz, 1993; Dunmyre et al., 2011; Hodgkin & Huxley, 1952; Terman et al., 2002; Wang et al., 2003), and the parameters that were varied were merely the maximal conductances of some ionic currents that vary among the various neuronal subtypes (Daou et al., 2013), as well as the synaptic conductances. Every model neuron is represented by ordinary differential equations for the different state variables as illustrated below.

Ion channels of model HVC neurons

We added a hyperpolarization-activated inward current conductance (I_H) to HVC_X and HVC_{INT} because it is responsible for the sag seen in these neurons (Daou et al., 2013; Dutar et al., 1998; Kubota & Saito, 1991; Kubota & Taniguchi, 1998), and we added a low-threshold T-type Ca^{2+} current (I_{CaT})conductance responsible for the post-inhibitory rebound firing seen in HVC_X and HVC_{INT} neurons (Daou et al., 2013). A small-conductance Ca^{2+}-activated K^+ current (I_{SK}) was added for HVC_{RA} and HVC_X neurons as it is responsible for the spike frequency adaptation feature that these two classes exhibit (Daou et al., 2013). For interneurons, we integrated a large magnitude of the delayed rectifier K^+ current conductance allowing these neurons to undershoot the resting membrane potential as seen experimentally (Daou et al., 2013; Dutar et al., 1998; Kubota & Saito, 1991; Kubota & Taniguchi, 1998). For HVC_{RA} neurons, we added an A-type K+ current that supports the delay to spiking seen in response to depolarizing current pulses (Daou et al., 2013; Kubota & Taniguchi, 1998; Mooney & Prather, 2005). High-threshold Ca^{2+} conductance was added to all classes of HVC neurons (Daou et al., 2013; Kubota & Saito, 1991; Long et al., 2010). In total, the model was designed to include spike-producing currents (I_K and I_{Na}), a high-threshold L-type Ca^{2+} current (I_{CaL}), a low-threshold T-type Ca^{2+} current (I_{CaT}), a small-conductance Ca^{2+} – activated K^+ current (I_{SK}), an A-type K^+ current (I_A), a hyperpolarization-activated current (I_H), and a leak current (I_L). The membrane potential of each HVC neuron obeys the following equations:

$$C_m \frac{dV_{RA}}{dt} = -I_L - I_K - I_{Na} - I_{CaL} - I_A - I_{SK} \quad (1)$$

$$C_m \frac{dV_X}{dt} = -I_L - I_K - I_{Na} - I_{CaL} - I_{CaT} - I_{SK} - I_H \quad (2)$$

$$C_m \frac{dV_{INT}}{dt} = -I_L - I_K - I_{Na} - I_{CaL} - I_{CaT} - I_H \quad (3)$$

where C_m is the membrane capacitance. The associated equations and parameters for each of the activation/inactivation gating variables for each ionic current are given in (Daou et al., 2013) and shown below. In total, every single model HVC_{RA}, HVC_X, and HVC_{INT} neuron had a total of 6, 8 and 7 ODEs, respectively, that govern their intrinsic dynamics. Every synaptic current that was integrated to any model neuron added a new ODE to the set of ODEs governing the membrane potential of the corresponding model neuron.

Voltage-gated ionic currents

The constant-conductance leak current is $I_L = g_L(V-V_L)$. The remaining voltage-gated ionic currents have non-constant dependent currents with activation/inactivation kinetics:

$$I_K = g_K n^4 (V - V_K) \quad (4)$$

$$I_{Na} = g_{Na} m_\infty^3(V) h (V - V_{Na}) \quad (5)$$

$$I_A = g_A a_\infty(V) e (V - V_K) \quad (6)$$

$$I_{CaL} = g_{Ca} s_\infty^2(V) \frac{Ca_{ex}}{1-e^{\frac{2FV}{RT}}} \quad (7)$$

$$\text{where } x_\infty(V) = \frac{1}{1+e^{\frac{V-\theta_x}{\sigma_x}}}, \quad x = m, a \text{ or } s \quad (8)$$

$$\text{and } \frac{dx}{dt} = \frac{x_\infty(V)-V}{\tau_x}, \; x = n, h \text{ or } e \quad (9)$$

where $x_\infty(V)$ for n and e is given by (8) and for h_∞ as follows

$$h_\infty(V) = \frac{\alpha_h(V)}{\alpha_h(V)+\beta_h(V)} \quad (10)$$

$$\text{where} \quad \alpha_h(V) = 0.128 e^{\frac{V+15}{-18}} \quad (11)$$

$$\text{and} \quad \beta_h(V) = \frac{4}{1+e^{\frac{V+27}{-5}}} \quad (12)$$

Low-voltage activated T-type calcium current

The low-voltage activated T-type Ca2+ current is described by the Goldman-Hodgkin-Katz formula:

$$I_{CaT} = g_{CaT} (a_T)_\infty^3(V)(b_T)_\infty^2(r_T) \frac{Ca_{ex}}{1-e^{\frac{2FV}{RT}}} \quad (13)$$

$$\text{where } a_{T_\infty}(V) = \frac{1}{1+e^{\frac{V-\theta_{a_T}}{\sigma_{a_T}}}} \quad (14)$$

$$\text{and } b_{T_\infty}(r_T) = \frac{1}{1+e^{\frac{r_T-\theta_b}{\sigma_b}}} - \frac{1}{1+e^{\frac{-\theta_b}{\sigma_b}}} \quad (15)$$

$$\text{with } \frac{dr_T}{dt} = \frac{r_{T_\infty}(V)-r_T}{\tau_{r_T}(V)} \quad (16)$$

$$\text{and } r_{T_\infty}(V) = \frac{1}{1+e^{\frac{V-\theta_{a_T}}{\sigma_{a_T}}}} \quad (17)$$

$$\text{and } \tau_{r_T}(V) = \tau_{r_0} + \frac{\tau_{r_1}}{1+e^{\frac{V-\theta_{r_{T_T}}}{\sigma_{r_{T_T}}}}} \quad (18)$$

Calcium-dependent Potassium current

The small conductance potassium current (I_{SK}) is modeled as

$$I_{SK} = g_{SK}\, k_\infty([Ca^{2+}]_i)(V - V_K) \quad (19)$$

$$\text{where } k_\infty([Ca^{2+}]_i) = \frac{[Ca^{2+}]_i^2}{[Ca^{2+}]_i^2 + k_s^2} \quad (20)$$

$$\text{and } \frac{d[Ca^{2+}]_i}{dt} = -f\,\varepsilon(I_{CaL} + I_{CaT}) + k_{Ca}([Ca^{2+}]_i - b_{Ca}) \quad (21)$$

Hyperpolarization-activated inward current

The hyperpolarization activated inward current's activation is modeled as in Destexhe and Babloyantz (1993) using a fast component (r_f) and a slow component (r_s) as follows:

$$I_H = g_H\,[k_r r_f + (1 - k_r)\,r_s](V - V_h) \quad (22)$$

The fast activation component is given by:

$$\frac{dr_f}{dt} = \frac{r_{f_\infty}(V) - r_f}{\tau_{r_f}(V)} \quad (23)$$

$$\text{where } r_{f_\infty}(V) = \frac{1}{1 + e^{\frac{V - \theta_{r_f}}{\sigma_{r_f}}}} \quad (24)$$

with its time constant τ

$$\text{with its time constant } \tau_{r_f}(V) = \frac{p_{r_f}}{\frac{-7.4(V+70)}{e^{\left(\frac{V+70}{-0.8}\right)} - 1} + 65\, e^{\left(\frac{V+56}{-23}\right)}} \quad (25)$$

The slow activation component obeys:

$$\frac{dr_s}{ds} = \frac{r_{s_\infty}(V) - r_s}{\tau_{r_s}} \quad (26)$$

$$\text{where } r_{s_\infty}(V) = \frac{1}{1 + e^{\frac{-(V - \theta_{r_s})}{\sigma_{r_s}}}} \quad (27)$$

Synaptic currents

In addition to the ionic currents above that orchestrate the internal dynamics of each HVC neuron, we integrated synaptic currents in order to reproduce the biological features of the voltage traces observed *in vivo*. Excitatory (AMPA) and inhibitory ($GABA_A$) synaptic currents were used to connect neurons inside each architecture based on the pharmacological dual synaptic connections as described by Mooney and Prather (2005). Each synaptic current represents the synaptic input(s) from the presynaptic cell(s) to the particular HVC model neuron, and is modeled as $I_{syn} = \sum_X I_{X \to Y}$ where $I_{X \to Y} = g_{X \to Y} s_{X \to Y}(V - V_{X \to Y})$. Here the summation is taken over the presynaptic HVC neurons where X represents a presynaptic cell, Y represents a postsynaptic cell, $V_{X \to Y}$ is the reversal potential for the synapse in the postsynaptic cell with $V_{X \to Y} = V_{AMPA}$ for excitatory input and $V_{X \to Y} = V_{GABA\text{-}A}$ for inhibitory input.

The model equations for the synaptic currents are the following, taken after (Destexhe et al., 1994; Varela et al., 1997).

$$I_{AMPA} = \overline{g_{AMPA}} s_{AMPA}(V - V_{AMPA})$$

$$I_{GABA-A} = \overline{g_{GABA-A}} s_{GABAA}(V - V_{GABA-A})$$

where s_{AMPA} and s_{GABAA} are given by

$$[T]_{pre} = \frac{T_{max}}{1 + \exp\left(\frac{V_{pre} - V_T}{K_p}\right)} \text{ and } \frac{d_s}{d_t} = a_r\,[T](1 - s) - a_d s$$

with $T_{max} = 1$, $K_p = 5$, $V_T = 2$. For $GABA_A$, $a_r = 5$ and $a_d = 0.18$, while for AMPA, $a_r = 1.1$ and $a_d = 0.19$.

We limited our synaptic currents' choices in all networks to AMPA (excitatory) and $GABA_A$ (inhibitory) without integrating NMDA and $GABA_B$ for the following reasons: 1) both AMPA and $GABA_A$ currents are voltage-dependent with simple activation kinetics that do not depend on

further parameters that are very hard to tune or calibrate (for example, NMDA current relies on Mg^{2+} concentration and $GABA_B$ on G-proteins dynamics, both which require additional ODEs and series of parameters that we don't know about in the HVC), 2) adding the additional synaptic currents do not have a significant contribution to the network dynamics we're building because the emphasis is on excitation and inhibition and we could convey the mechanisms we envision that orchestrate each network with these two currents solely. Therefore, model HVC_{RA} neurons send their excitatory afferents to other HVC_{RA} neurons as well as to HVC_{INT} neurons via AMPA currents. Model HVC_{INT} neurons send their inhibitory afferents to both HVC_{RA} and HVC_X neurons via $GABA_A$ currents. And lastly, model HVC_X neurons excite HVC_{INT} neurons via AMPA currents.

Desired network activity

Our aim here is to generate the optimal and desired network activity that's generated by the three classes of HVC neurons during singing. Therefore, we focused on model parameters and their underlying mechanisms that play key roles in 1) reproducing the patterns without breaking the sequence of activity propagation and 2) generate biologically realistic traces for each class as shown using intracellular recordings *in vivo* in a way to maintain spike shapes, burst patterns, rebound firing/bursting, subthreshold oscillations, etc … In a nutshell, the behavior of the network was considered desired and "good" if the model voltage traces for the total populations in each of the three classes of HVC neurons in the network matched the following: 1) the time-locked and characteristic bursting of HVC_{RA} neurons (3-6 spikes for a ~10 ms duration), with spikes riding on a plateau, 2) HVC_X neurons eliciting 1-4 bursts (4-9 spikes per burst) that are also time-locked and that are mostly rebound bursts from inhibition (Lewicki, 1996; Mooney, 2000), 3) HVC_{INT} neurons exhibiting tonic activation with spiking and bursting throughout the song, and 4) spike frequency, spike amplitude, sags and/or rebound upon inhibition, resting membrane potential and other known features of the intrinsic properties of the three classes of HVC neurons exhibited for each of the classes that exhibit them (Daou et al., 2013).

Maximal and synaptic conductances variations

Automated adjustment of model parameters was performed to qualitatively reproduce desired membrane potential trajectories, as described next. Fixed parameter values for HVC neurons used in the simulations are given in **Table 1**. Parameters that vary between the different model neurons are shown in **Figure 2-A**.

Some maximal conductances were fixed while others were allowed to vary. We fixed g_{Na} and g_K for each class of the HVC neurons to values that had been shown earlier to accurately fit the spike morphologies (upstrokes and downstrokes of action potentials, plateaus, etc…) in response to applied current given *in vitro* (Daou et al., 2013). For example, HVC_{INT} neurons' spikes exhibit a relatively large undershoot of the resting membrane potential, while HVC_X and HVC_{RA} spikes ride on a plateau with characteristic properties (Daou et al., 2013). We also fixed the value of g_{CaL} because we could achieve the same accuracy of fitting by varying g_{SK}, and so could not distinguish between the two.

The four key conductances in our model that played crucial roles in controlling not only the intrinsic properties of the HVC neurons they're expressed in but also in shaping overall network activity and sequence propagation are g_{SK}, g_h, g_A and g_{CaT}. As a recap, g_{SK} is expressed in HVC_X and HVC_{RA}, g_H and g_{CaT} in HVC_X and HVC_{INT}, and g_A in HVC_{RA} only (Daou et al., 2013). Random variations in these four parameters were performed to qualitatively reproduce membrane potential trajectories of the three classes of HVC neurons as seen firing when the bird is singing.

In a previous study, Daou and Margoliash (2020) showed that intracellular recordings from X-projecting neurons in adult zebra finch brain slices share similar spike waveform morphologies, with modeling indicating similar magnitudes of their principal ion currents. To that end, we fixed in our network the intrinsic properties of the population of HVC_X neurons to the same values.

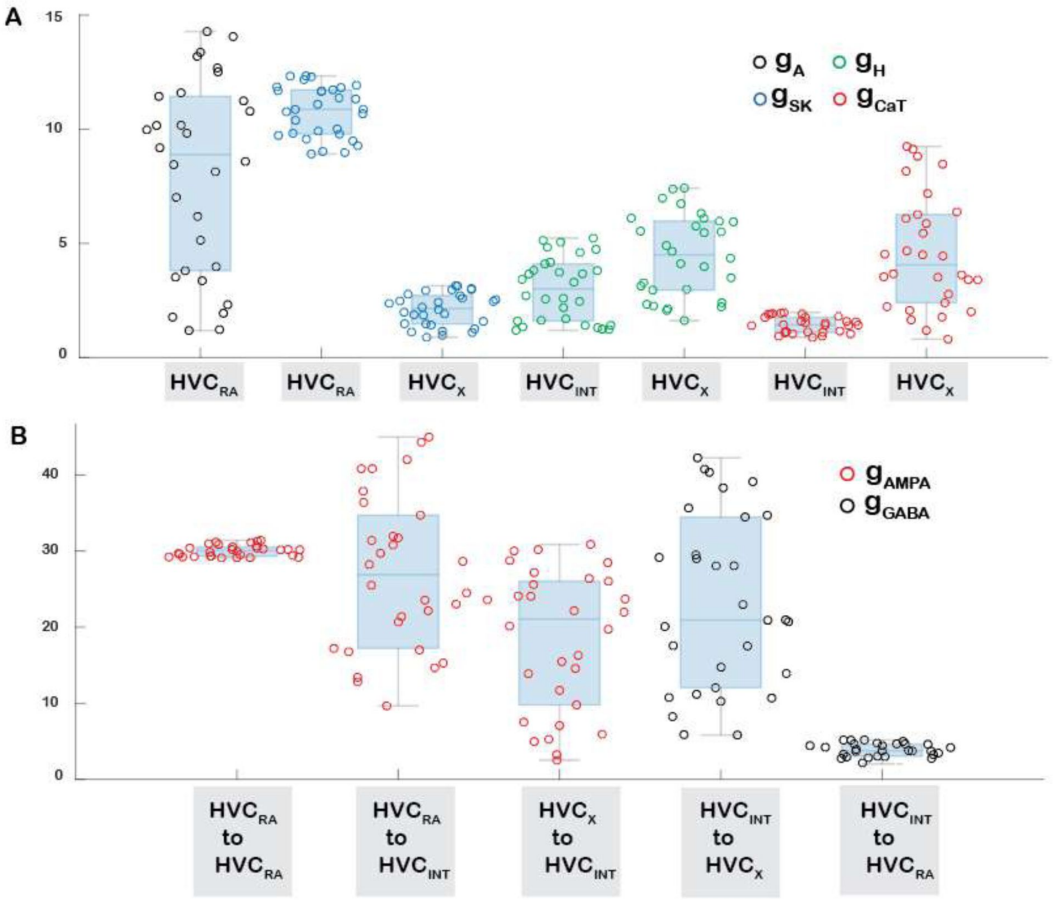

Figure 2.

Box plots showing the ranges of ionic and synaptic currents that were allowed to vary while maintaining robust network propagation and biologically realistic in vivo behavior of all HVC neuronal classes.

A. The ionic conductances that were varied are g_A of HVC_{RA}, g_{SK} of HVC_{RA} and HVC_X, g_h and g_{CaT} of HVC_{INT} and HVC_X. The shown ranges reflect values whereby each neuron class is able to maintain realism in terms of electrophysiological behavior and network properties. **B.** Ranges of values of synaptic conductances that connect two classes of HVC neurons while conserving sequential activity propagation and the general network activity.

Parameter	Value	Parameter	Value
V_L	$-70\ mV$	θ_{a_T}	$-65\ mV$
V_K	$-90\ mV$	θ_b	$0.4\ mV$
V_{Na}	$50\ mV$	θ_{r_T}	$-67\ mV$
V_{Ca}	$85\ mV$	$\theta_{r_{r_T}}$	$68\ mV$
V_H	$-30\ mV$	σ_m	$-5\ mV$
g_L	$2\ nS$	σ_n	$-5\ mV$
g_{Ca}	$19\ nS$	σ_s	$-0.05\ mV$
τ_n	$10\ msec$	σ_a	$-10\ mV$
τ_{hp}	$1000\ msec$	σ_e	$5\ mV$
τ_e	$20\ msec$	σ_{r_f}	$5\ mV$
τ_h	$1\ msec$	σ_{r_s}	$25\ mV$
τ_{r_s}	$1500\ msec$	σ_{a_T}	$-7.8\ mV$
τ_{r_0}	$200\ msec$	σ_b	$-0.1\ mV$
τ_{r_1}	$87.5\ msec$	σ_{r_T}	$2\ mV$
θ_m	$-35\ mV$	$\sigma_{r_{r_T}}$	$2.2\ mV$

Table 1.

Fixed parameter values used in all simulations.

$\boldsymbol{\theta_n}$	$-30\ mV$	f	0.1
$\boldsymbol{\theta_s}$	$-20\ mV$	$\boldsymbol{\varepsilon}$	$0.0015\ pA^{-1}$ microM $msec^{-1}$
$\boldsymbol{\theta_a}$	$-20\ mV$	$\boldsymbol{k_{Ca}}$	$0.3\ msec^{-1}$
$\boldsymbol{\theta_e}$	$-60\ mV$	$\boldsymbol{b_{Ca}}$	$0.1\ micro\ M$
$\boldsymbol{\theta_{r_f}}$	$-105\ mV$	$\boldsymbol{k_s}$	$0.5\ micro\ M$
$\boldsymbol{\theta_{r_s}}$	$-105\ mV$	$\boldsymbol{p_{r_f}}$	100
$\boldsymbol{g_{Na_{HVC_{RA}}}}$	$300\ nS$	$\boldsymbol{g_{K_{HVC_{RA}}}}$	$150\ nS$
$\boldsymbol{g_{Na_{HVC_X}}}$	$450\ nS$	$\boldsymbol{g_{K_{HVC_X}}}$	$80\ nS$
$\boldsymbol{g_{Na_{HVC_{INT}}}}$	$800\ nS$	$\boldsymbol{g_{K_{HVC_{INT}}}}$	$1200\ nS$

Table 1. (continued)

Therefore, the automated variations in the conductances held for HVC_X neurons were done at the population level by varying a corresponding ionic conductance value (say, g_{SK}) and setting its value to all of the HVC_X population. We also checked the effects of removing this constraint in **Figure 13**, that is, allowing the intrinsic properties of HVC_X neurons to vary like other parameters.

We first manually selected the four key conductances to default values that generate the desired behavior of the network as described in the previous section. Network robustness to varied maximal conductances as well as the legitimate ranges for each maximal conductance was determined by simulating the network many times, each time with a random variation in the maximal conductance about its default value. The network response was considered accurate if the network generated sequential bursting and all of the desired features described earlier. The range of variation of the randomly-varying parameter was increased or decreased randomly up until the point that the network ceased to be accurate.

The variation in parameters was done at the population level (setting the maximal conductance for all neurons of the same class to a single value and randomly changing that value for all), well as on the individual neuronal level (varying the maximal conductance for one neuron at a time of the same class while fixing the others to their default values). This is different for the HVC_X parameters, where the corresponding conductances at the population and the neuronal levels are considered the same since we assumed same intrinsic properties as described earlier. If any of the simulations generated networks where any of the HVC_{RA} neurons elicit bursts exhibiting spikes outside the 3-6 number of spikes range or duration of any burst longer than 10 ms, then we ignore that parameter value. Similarly, if any of the simulations generate networks where any of the HVC_X neurons eliciting more than 4 bursts, individual bursts exhibiting spikes outside the 4-9 spikes/burst range, then the corresponding parameters are ignored. Moreover, we also ignore parameters that generate unrealistic intrinsic properties of individual HVC neurons; for instance, if the resting membrane potentials of individual HVC neurons were outside the reported ranges (Daou et al., 2013), if HVC_X and HVC_{INT} neurons failed to generate sags and rebounds (depolarization or bursting) in response to inhibition, or if spikes' amplitudes were not realistic (HVC_X and HVC_{RA} spikes not riding on plateaus or HVC_{INT} spikes not undershooting the RMP). We realize this might be inducing tough constraints on the selection of the parameters limiting the space for which the conductances are allowed to vary, but we opted for this method in order to generate the optimal ranges in which intrinsic and synaptic conductances are able to reproduce the biophysically realistic firing patterns seen during singing. We therefore ended up with lists of ranges for each conductance that was varied and in each class of HVC neuron, such that the desired network activity is maintained. **Figure 2-A** shows the ranges for each maximal conductance that had been allowed to vary for the three classes of HVC neurons, while maintaining robust network propagation and biologically realistic in vivo behavior.

Similar to what was done with the maximal ionic conductances, we conducted automated and random variations for all synaptic conductances in the model (no synaptic conductance was fixed). **Figure 2-B** reports the ranges of the synaptic conductances that were able to maintain the robustness of network propagation and the general *in vivo*-like desired behavior of all neuronal classes. All synaptic conductances showed considerable ranges during which sequential activity is propagated and the overall desired network activity is maintained, with the exception of the GABA conductance from HVC_{INT} to HVC_{RA} ($g_{GABAINT \rightarrow RA}$). Increasing $g_{GABAINT \rightarrow RA}$ to larger magnitudes would induce an inhibition in the HVC_{RA} pushing its voltage below its resting membrane potential (due to the dense bursting and firing in HVC_{INT}), and this is not realistic because it's been shown that during singing HVC_{RA} neurons ride on a depolarizing plateau throughout the song (Long et al., 2010). Moreover, while the intrinsic properties of HVC_X neurons were set to the same values, the synaptic parameters associated with each HVC_X neuron (afferent and efferent) were allowed to vary from one neuron to another.

Results

Adult zebra finches generate intricate songs composed of sequences of distinct song elements, each characterized by a stereotypical acoustic pattern across every rendition of song. The neural circuitry that governs this behavior consists of HVCRA neuronal population where each emits a single and stereotyped 6-10 ms burst during each rendition of song, HVCX neurons eliciting 1-4 bursts that are similarly time locked to vocalizations, and HVCINT neurons that tend to burst densely throughout song. Intrinsic and synaptic mechanisms that orchestrate these neurons' behaviors are well known (Daou et al., 2013; Kornfeld et al., 2017; Mooney & Prather, 2005). We next describe the steps of building our biophysical network model to describe this ongoing behavior in the following order: 1) tuning the synaptic parameters to fit the dual-intracellular recording traces collected experimentally by Mooney and Prather (2005) as well as Kosche et al (2015), and then 2) describing the network components that are essential for the patterned output of the system, as well as the internal dynamics of the network that govern the strength and duration of individual bursts, the duration of silent gaps between bursts, sparseness versus tonicity, the interplay between excitation and inhibition, role of intrinsic properties and so on that explain how the firing activity of the three classes of HVC neurons propagate through the network in sequential manner.

Tuning synaptic parameters

We initiated our HVC network modeling study calibrating the synaptic parameters (excitatory and inhibitory currents' activation/inactivation constants, etc..) by reproducing the voltage traces elicited by the dual intracellular recordings from identified pairs of HVC neurons in brain slices conducted by Mooney and Prather (2005). While we are using off-the-shelf synaptic currents from the literature (Destexhe et al., 1994; Varela et al., 1997), we needed to make sure that the synaptic parameters used can replicate the dual synaptic connectivity patterns (strengths of excitation/inhibition, magnitudes of voltage deflections and other trace morphologies). Mooney and Prather's findings revealed robust disynaptic feedforward inhibition from HVCRA to HVCX neurons (mediated by HVCINT neurons), potent monosynaptic excitation from HVCRA and HVCX to HVCINT neurons (via NMDA and AMPA currents), and substantial monosynaptic inhibition from HVCINT neurons to HVCRA and HVCX (via GABA currents).

Figure 3 displays the dual intracellular recordings conducted by Mooney and Prather (left column) as well as the mathematical model replications (right column) after the synaptic parameters' calibration. DC-evoked action potentials in HVCRA neurons trigger inhibitory postsynaptic potentials (iPSPs) in HVCX neurons (**Fig. 3-A1**), as well as fast depolarizing postsynaptic potentials (dPSP) in HVCINT neurons (**Fig. 3**-B1). To replicate the effects of stimulating HVCRA neurons onto the other two classes of HVC neurons, we connected one HVCRA neuron to excite one HVCINT neuron via an AMPA current. The HVCINT neuron in its turn was connected with one HVCX neuron via a GABA current, thereby making a di-synaptic pathway from HVCRA to HVCX. DC-evoked action potentials in the model HVCRA neuron (brief ~10 ms depolarizing current pulses (0.5 nA, similar to what Mooney and Prather applied to HVCRA neurons) evoked a fast-depolarizing postsynaptic potential (dPSP) in the corresponding model HVCINT neuron (**Fig. 3**-B2) as well as inhibitory postsynaptic potential (iPSP) in the corresponding model HVCX neuron (**Fig. 3**-A2) mediated via HVCINT. Similarly, DC-evoked action potentials in HVCINT neurons generate fast iPSPs in HVCX neurons (**Figures 3**-C1, D1). The unequal magnitude of the four sags elicited in the HVCX neuron (due to the four brief stimuli) and the large sag after the stimuli ends (**Fig. 3**-C1), as well as the jagged long sag in response to the repetitive action potentials elicited by the HVCINT neuron (**Fig. 3**-D1) is probably due to the fact that the corresponding HVCX neurons are receiving multiple synaptic inputs from neurons other than the neurons being stimulated by Mooney and Prather, which adds to the underlying nonlinearities of the responses

being recorded. Model HVCINT and HVCX neurons were connected and synaptic parameters were calibrated to generate similar waveforms by giving brief ~10 ms depolarizing current pulses of 0.5 nA to HVCINT (**Fig. 3**-C2), or giving a DC-pulse of 0.5 nA for 500 ms (**Fig. 3**-D2). In the model, the sag seen in the HVCX neuron response is due to the build-up of the H-current as the model HVCINT neurons continues firing, exerting its inhibition onto the HVCX neuron. Finally, model HVCX-HVCINT monosynaptic connectivity (**Fig. 3**-E2) was calibrated to match the experimental findings (**Fig. 3**-E1).

Network Architecture: Non-sequential random sampling in HVC

We next describe the activity patterns generated by our network model, and explain how the firing activity of the three classes of HVC neurons propagate through the network in sequential bursts of activity. The network developed is composed of chains of HVC subnetworks or microcircuits, each with its own intrinsic dynamics. The microcircuit represents a basic architectural unit that encodes for a syllable or a sub-syllabic segment (SSS) in the motif (**Fig. 4**). Each neuron in a microcircuit is representative of a neural population. In other words, a model neuron (belonging to any class) firing is representative of a population of that neuronal class firing, which could be many neurons of the same class exhibiting very similar intrinsic and synaptic properties leading to their firing at the same time. We refer here to "microcircuits" in a more functional sense, rather than rigid, isolated spatial divisions (Cannon et al. 2015). A microcircuit in our model reflects the local rules that govern the interaction between all HVC neuron classes within the broader network, and that are essential for proper activity propagation.

The number of microcircuits in the chain determines the number of SSSs in the motif. We envision the HVC to be composed of many copies of such microcircuit chains that are associated with SSSs with roughly synchronized activity. The duration of the sub-syllabic segments need not be the same; therefore, the number of neurons that each microcircuit encompasses need not be equal as we will see next. The network is comprised of a total pool of HVCRA neurons (120 neurons, red circles), a pool of interneurons (50 neurons, black circles) and a pool of HVCX neurons (50 neurons, blue circles), thereby maintaining a 2:1:1 proportionality factor across the populations of HVCRA: HVCINT: HVCX as reported earlier (Kornfeld et al., 2017; Wild et al., 2005). The total number of neurons in the pool is arbitrary and can be made larger, but we limited it to these values given the huge number of ODEs that are being simulated (~2000 ODEs). **Figure 4-A** shows the network diagram illustrating three sample microcircuits encoding for three sub-syllabic segments (SSSi-1, SSSi, and SSSi+1) in sequence. Each microcircuit (enclosed by a gray oval) is made up of a number of HVCRA neurons (red circles) and a number of HVCINT neurons (black circles), all selected randomly from their corresponding pools, as we will describe next. In our model, we limited the number of microcircuits to twenty (i.e., the motif is encoded by twenty sub-syllabic segments), but this number is also arbitrary and can be made larger or smaller.

Network organization: The total pool of HVCRA neurons is comprised of smaller groups of HVCRA neurons, the number in each group of which is chosen randomly from the pool (red background circles in each gray oval). Each group of HVCRA neurons belongs to a unique microcircuit and no HVCRA neuron is allowed to be part of more than one microcircuit for reasons described next. Since we set the motif to be represented by twenty microcircuits in our illustration, HVCRA neurons were recruited to their corresponding microcircuits randomly, with each microcircuit allowing a random number (3 – 10) neurons of the RA-projectors to belong to it. In addition to that, the numbers of HVCINT neurons (black background circles) that a microcircuit exhibit is a random number between 1 and 4, as well as the number of HVCX neurons (blue background circles) in each microcircuit is random between 1 and 4, where the individual neurons are selected arbitrarily one neuron at a time from their corresponding pools. Each HVCINT neuron can belong to a single microcircuit and similarly each HVCX neuron can belong to a single microcircuit for reasons described next.

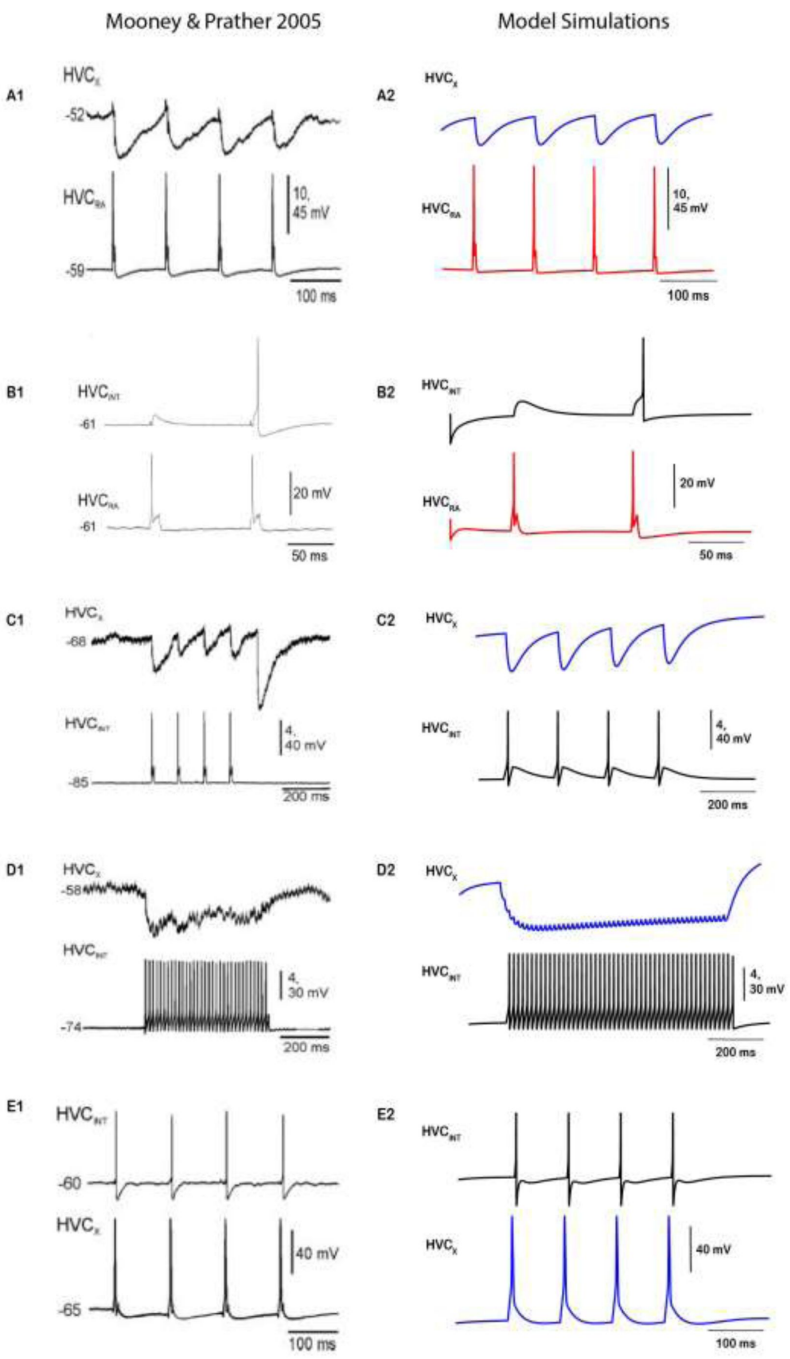

Figure 3.

Model output compared to experimental results obtained by Mooney and Prather (2005).

DC-evoked action potentials in HVC_{RA} neurons trigger iPSPs in HVC_X neurons (**A1**) as well as fast dPSPs in HVC_{INT} neurons (**B1**). Brief (~10 ms) depolarizing current pulses (0.5 nA) applied to model HVC_{RA} neuron (same values used as by Mooney and Prather (2005)) evokes similar responses in the corresponding model HVC_X (**A2**) and model HVC_{INT} (**B2**) neurons. DC-evoked action potentials in HVC_{INT} neurons generate fast iPSPs in HVC_X neurons (**C1**, **D1**). Similar responses were elicited in model HVC_X neurons when model HVC_{INT} neuron was stimulated by brief (10 ms) depolarizing pulses (0.5nA) (**C2**) or when it was given a DC-pulse of 0.5 nA for 500 ms (**D2**). Finally, HVC_{INT} neurons elicit fast dPSPs when HVC_X neurons are injected with 10 ms pulses of 0.5 nA current (**E1**), which was simulated in the model (**E2**). In this and subsequent figures (unless otherwise specified), HVC_X neurons' traces are represented in blue, HVC_{RA} neurons in red, and HVC_{INT} neurons in black. Panels in the left column adopted from Mooney and Prather (2005).

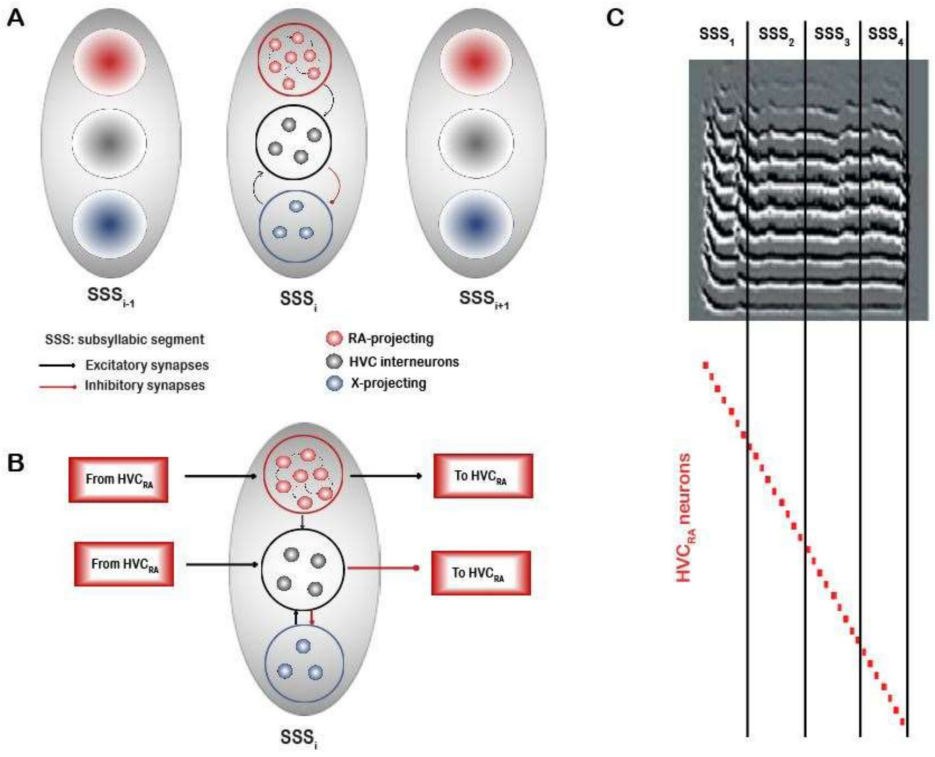

Figure 4.

Cartoon diagram illustrating the network architecture configuration.

A. Each grey oval represents a microcircuit encoding for a sub-syllabic segment (SSS). The number of microcircuits is envisioned to be equal to the number of SSSs representing the song. Each microcircuit contains a number of HVC_{RA}, HVC_X and HVC_{INT} neurons selected randomly from the total pool of neurons (see text). **B**. Within each microcircuit, HVC_{RA} neurons are connected to each other in a chain-like mode and they send excitatory afferents to HVC_{INT} neurons in the same and other microcircuits, selected randomly. HVC_{INT} neurons send GABAergic synapses onto HVC_X neurons in the same microcircuit only as well as to HVC_{RA} neurons in any other random microcircuit except the microcircuit they belong to. Finally, HVC_X neurons send excitatory afferents to HVC_{INT} neurons in the same microcircuit. Activity starts by a small DC pulse to the first HVC_{RA} neuron in the first microcircuit. Activity propagates from one microcircuit to another by excitatory coupling between the last HVC_{RA} neuron in microcircuit i and the first HVC_{RA} neuron in microcircuit i+1. **C.** During singing, the propagation of activity unfolds across the chain of microcircuits, such that neurons belonging to microcircuit x gets activated and encode for SSS_x.

Synaptic Connectivity: Within each microcircuit, HVCRA neurons are selected randomly, one after the other, to send AMPA excitatory synapses to each other in a chain-like mode. Specifically, if there are m HVCRA neurons recruited to belong to microcircuit i (where m is the random number generated between 3 and 10 in this case), a neuron from the m is first selected randomly and designated as the first neuron in the chain ($HVC^{i}_{RA_1}$). After that, a second neuron ($HVC^{i}_{RA_2}$) from the remaining $m - 1$ is selected randomly and an AMPA synapse is connected from $HVC^{i}_{RA_1}$ to $HVC^{i}_{RA_2}$. Similarly, a third neuron ($HVC^{i}_{RA_3}$) is selected randomly from the remaining $m - 2$ neurons and an AMPA synapse is connected from $HVC^{i}_{RA_2}$ to $HVC^{i}_{RA_3}$, and so on, until the HVCRA neurons in every microcircuit are connected together (**Fig. 4A**, small red circles in each microcircuit).

Each HVCINT in a microcircuit was assigned a random number (between 3 and 8) of excitatory AMPA connections from the HVCRA neurons in the same microcircuit it belongs to, as well as from HVCRA neurons in the other microcircuits (**Fig. 4B**). In their turn, each HVCINT neuron sends a random number (between 2 and 4) of GABAergic inputs to HVCRA neurons, chosen arbitrarily from any microcircuit in the chain except the microcircuit that the HVCINT neuron belongs to, due to the following reason: if HVCINT inhibits HVCRA in the same microcircuit, some of the HVCRA bursts in the microcircuit might be silenced by the dense and strong HVCINT inhibition breaking the chain of activity. However, if HVCINT inhibits HVCRA in any other microcircuit, activity is ensured to propagate because the HVCINT inhibition of the corresponding HVCRA would arrive at times that are not the "assigned" times of the HVCRA to elicit their ultra-sparse code (Hahnloser et al., 2002).

Unlike HVCRA, HVCINT neurons belonging to a particular microcircuit can burst at times other than the moments when the corresponding encoded SSS is being "sung"; however, we chose to house interneurons within microcircuits for the mere fact that any given interneuron cannot inhibit any given HVCRA neuron, rather there are some "rules of engagement" where we ensure that no inhibition arrives to any HVCRA neuron while it's eliciting its burst of activity (**Fig. 4B**). In other words, what makes a particular interneuron belong to this microcircuit or the other is merely the fact that it cannot inhibit HVCRA neurons that are housed in the microcircuit it belongs to for the reasons described. In this regard, this arrangement is similar to the Cannon et al (2015) model in the context of structured inhibition amid the ongoing feedforward excitation.

At the HVCX side, each X-projecting neuron excites via AMPA currents a random selection (1 – 3) of HVCINT neurons that belong to the same microcircuit, and in their turn, each HVCINT neuron inhibits via GABA synapses a random selection (1-2) of HVCX neurons in the same microcircuit (**Fig. 4B**). These numbers are again arbitrary, but we limited the number of connections from HVCINT to HVCX due to that fact that X-projecting neurons in our model fire upon rebound from inhibition, and the more inhibitory inputs they receive, the more rebound bursts they elicit, which is not realistic since HVCX neurons are known to elicit 1 – 4 bursts during singing (Fujimoto et al., 2011; Kozhevnikov & Fee, 2007), which is what we achieved with this number of synapses. HVCX neurons were selected to be housed within microcircuits and their synapses connecting to interneurons within the same microcircuit due to the following reason: if an HVCX neuron belonging to microcircuit i sends excitatory input to an HVCINT neuron in microcircuit j, and that interneuron happens to select an HVCRA neuron from microcircuit i as its afferent inhibitory connection (via random sampling), then the propagation of sequential activity will halt, and we'll be in a scenario similar to what was described earlier for HVCINT neurons inhibiting HVCRA neurons in the same microcircuit. Similarly, if an HVCINT neuron in microcircuit i inhibits an HVCX neuron in another microcircuit j, and that HVCX neuron excites an interneuron that synapses onto an HVCRA from microcircuit i, then sequential activity might be disrupted.

While HVCRA neurons are connected to each other in each microcircuit in a chain-like mode as described earlier, the microcircuits interact with each other via the projections from the last HVCRA in a microcircuit i to the first HVCRA in a following microcircuit $i + 1$. The network is kick-started by a stochastic DC input to HVC^1, that is, only HVC^1 receives input from outside HVC. The

propagation of sequential activity along with the realistic firing of the three classes of HVC neurons is maintained and orchestrated by HVC's intrinsic and synaptic processes without relying on extrinsic inputs as shown next (**Figures. 5-11**).

Sequential propagation of HVCRA activity

The activity patterns that RA-projecting neurons of this network display are illustrated in **Figure 5**. HVCRA neurons burst extremely sparsely generating at most a single burst per simulation (song motif) and with different HVCRA neurons bursting at different times in the song. HVCRA bursts had a duration of 8.12 ± 0.89 ms, and comprised of 4.76 ± 0.48 spikes. The inset of **Fig. 5** shows the delay from the onset of the first spike in an HVCRA neuron to the onset of the first spike in the next HVCRA it synapses to. This duration is controlled by two factors: 1) the magnitude of the AMPA conductance, with larger magnitudes corresponding to shorter delays and vice versa (**Fig. 6A**). In short, the faster the AMPA current is (modeled as larger magnitude in the *gAMPA* parameter that connects two HVCRA neurons), the shorter the delay between the successive HVCRA bursts. 2) the magnitude of the A-type K^+ current conductance (g_A) with larger magnitudes corresponding to longer delays (**Fig. 6B**). This conductance increases rapidly on depolarization due to I_A's fast activation. The rapid increase in g_A halts after a few milliseconds and switches to a slow decrease that is due to the slow inactivation that this current exhibit. The slow decrease is reflected in the voltage trace as a slow depolarization in the membrane potential (encoding for the delay to spiking), and this allows the model HVCRA neuron to eventually escape the inhibition produced by I_A and fire its delayed burst.

The number of spikes in HVCRA neurons and the strength of the burst is controlled by three factors: 1) the strength of the AMPA conductance itself where stronger excitatory coupling corresponds to larger number of spikes (**Fig. 6A**), 2) the A-type K^+ conductance where larger magnitudes of the conductance reduce the general excitability of the HVCRA neuron and limit its number of spikes (**Fig. 6B**), and 3) the interplay between the L-type Ca^{2+} (g_{CaL}) and the Ca^{2+}-dependent K^+ (g_{SK}) conductances that control the strong adaptation which these neurons exhibit (Daou et al., 2013). In short, intracellular Ca^{2+} (due to *ICaL*) accumulates during the HVCRA burst. This result in a buildup of Ca^{2+}-activated K^+ current (I_{SK}) that terminates the HVCRA burst, which in turn terminates any burst in a post-synaptic neuron since HVCRA can no longer provide excitation.

The propagation of sequential bursting in HVCRA neurons halts and the chain of HVCRA activity is broken if any of the following is satisfied: 1) if an AMPA conductance for any of the HVCRA's that connects it to the next HVCRA in its chain is small enough such that it's not able to elicit sufficient excitability on the postsynaptic side, 2) if a g_A conductance (**Fig. 7A**) or a g_{SK} conductance (**Fig. 7B**) in any of the HVCRA's is large enough (mimicking an up-regulation in the corresponding channel) to eliminate the corresponding HVCRA's burst. Therefore, in order to generate accurate HVCRA bursting patterns that maintain the sequential propagation of neural activity, accurate number of spikes and delays between spikes across the population of HVCRA's in all microcircuits, as well as the general intrinsic properties of the HVCRA neurons' spike morphologies (see Methods), both intrinsic and synaptic constraints are needed with key roles in this process for the A-type K^+ and the Ca^{2+}-dependent K^+ currents that HVCRA model neurons exhibit, as well as the AMPA currents connecting the HVCRA population together within and across microcircuits. Recall that we envision each HVC neuron of any class in our model as a representative of a neural population of the same class that exhibits the same intrinsic as well as afferent and efferent synaptic connectivity. Therefore, in **Fig. 7 and the** subsequent figures (10,12 and 13) where we show disruption of sequential activity due to changes in synaptic or intrinsic properties of HVC neurons, the modeled synaptic/intrinsic changes to the selected neurons shown are envisioned to be changes applied to the whole neural population encoded by our model neuron. In other words, disrupting the properties of a single neuron within that neural population will not cause harm to the propagation of activity due to what could be thought of as homeostatic mechanisms of the

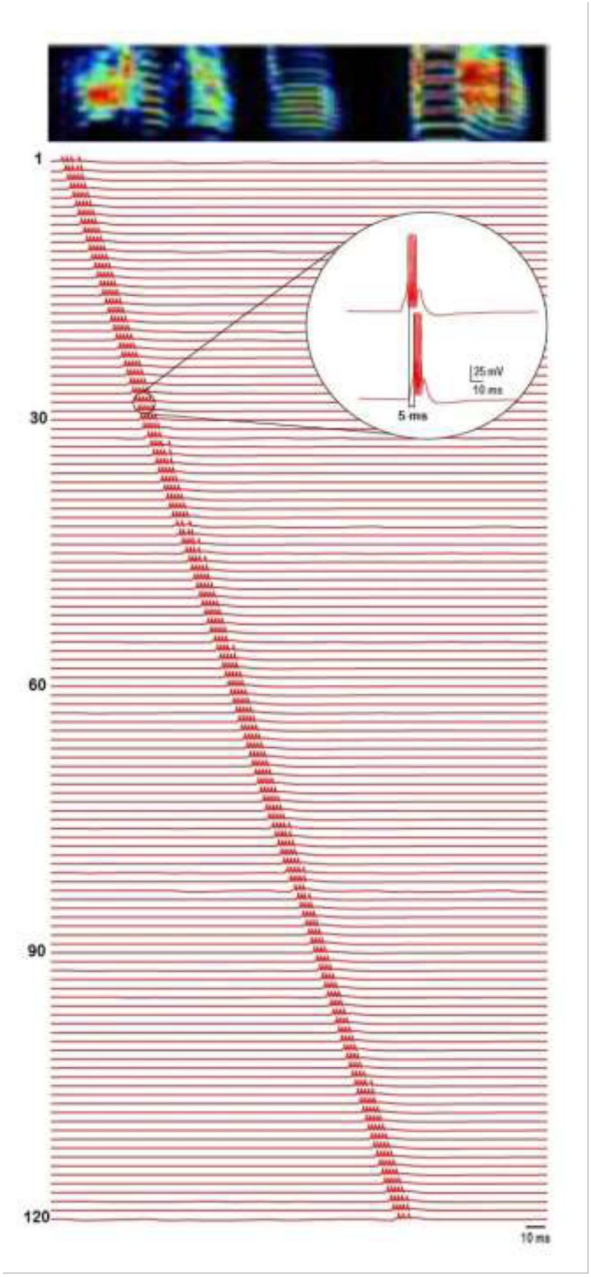

Figure 5.

Spiking patterns of 120 HVC_{RA} neurons (labeled with numbers) showing the propagation of sequential activity.

The neural traces are aligned by the acoustic elements of a spectrogram from an exemplar bird's song illustrating the firing of HVC_{RA} neurons with respect to ongoing part of a song. The inset shows a zoomed version of two subsequent HVC_{RA} neurons firing patterns illustrating the delay between their individual bursts.

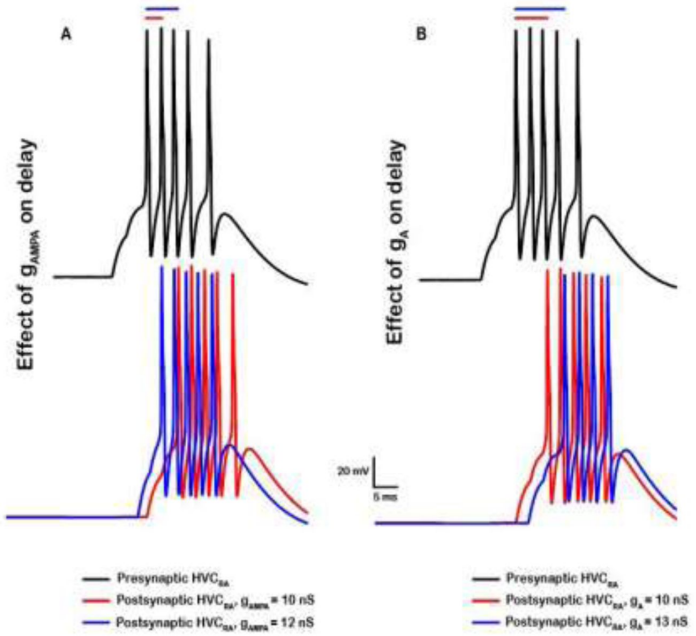

Figure 6.

Effects of the AMPA synaptic conductance and A-type K^+ conductance on the delay between two successive HVC_{RA} bursts.

A. Presynaptic model HVC_{RA} neuron (top, black) is connected to a postsynaptic model HVC_{RA} neuron and the corresponding AMPA excitatory conductance (g_{AMPA}) was increased from 10 nS (bottom, red) to 12 nS (bottom, blue), while keeping all other parameters fixed. Increasing g_{AMPA} reduce the delay between the peaks of the pre– and post-HVC_{RA}'s first spikes and increase the number of spikes in the postsynaptic neuron. **B**. Larger magnitudes of the A-type K^+ conductance (g_A) leads to longer delays to spiking. While keeping all intrinsic and synaptic parameters fixed (g_{AMPA} = 10), increasing g_A from 10 nS (bottom, red) to 13 nS (bottom, blue) delayed the onset to spiking and reduced the number of spikes. Bars on the top shows the duration in ms between the peak of first action potential in the presynaptic neuron to the peak of the first action potential in the postsynaptic neuron.

network (Golowasch et al., 1999; Marder & Goaillard, 2006; Williams et al., 2013). This redundancy within the population allows the propagation of activity to be maintained. It is an important feature of our model and is consistent with biological observations where neural populations exhibit robust collective behavior and the loss of a single neuron does not result in a major disruption of network activity.

Bursting patterns of HVCINT and HVCX neurons

The activity patterns that HVCINT neurons exhibit in our network architecture are illustrated in **Figure 8A** (shown here for 10 HVCINT neurons). In contrast to the sparse activity in RA-projecting neurons, HVC interneurons generate multiple bursts and spike densely as reported during the song (Hahnloser et al., 2002). The number of bursts each HVCINT neuron exhibits as well as the strength of each burst is controlled by network and synaptic mechanisms as described next (**Figures. 9**, 10). HVCX neurons in their turn generate 1 – 4 bursts per song motif (**Fig. 8B**, shown here for 10 HVCX neurons) similar to experimental results (Fujimoto et al., 2011; Hahnloser et al., 2002). Similarly, the number of bursts and strength of each HVCX burst depends on a set of synaptic and intrinsic mechanisms, illustrated in **Figures 11** and **12**. HVCX neurons differed in the number of bursts and the number of spikes per burst rendering the results more realistic.

Dense bursting in HVCINT

The random connections from HVCRA and HVCX neurons to HVCINT as well as the multiple bursts HVCINT and HVCX exhibit in this network are illustrated in **Figure 9** by highlighting a sample interneuron (HVC_{INT}^{10}). Here the firing patterns of HVC_{INT}^{10} in addition to all HVCRA and HVCX neurons that connect to it are shown. HVC_{INT}^{10} received random synaptic inputs from HVC_{RA}^{11}, HVC_{RA}^{32}, HVC_{RA}^{83} and HVC_{RA}^{120} neurons, as well as from X-projecting neurons HVC_{X}^{7}, HVC_{X}^{8} and HVC_{X}^{9} in the same microcircuit it belongs to. Notice that each HVCRA neuron (which happen to belong to separate microcircuits in this case), bursts only once as reported experimentally (Hahnloser et al., 2002). HVC_{INT}^{10} generates multiple bursts as well as spike sparsely. Each of the HVC_{INT}^{10} bursts are aligned with one of the bursts in HVCRA and/or HVCX neurons due to excitatory coupling.

The number of bursts an HVCINT neuron exhibits is largely determined by the number of bursts that each HVCRA and each HVCX neuron that synapses onto that interneuron exhibits. In other words, the larger the number of bursts that a population of HVCRA and HVCX that connects to an interneuron exhibit, the larger the number of bursts elicited in the interneuron. The strength of the bursts in HVCINT neurons is determined by two factors: 1) the strength of the excitatory synaptic conductance from HVCRA and/or HVCX to HVCINT, with stronger bursts in HVCINT corresponding to larger magnitudes of gAMPA from HVCRA and/or HVCX onto the interneuron, 2) the number of spikes/bursts in HVCRA and HVCX that are aligned and occur simultaneously at the HVCINT synapses. For example, the asterisk shown in **Figure 9** under the HVC_{INT}^{10} spike train highlights a stronger burst (compared to the rest of the spiking pattern) because HVC_{RA}^{83}, HVC_{X}^{7}, HVC_{X}^{8} and HVC_{X}^{9} neurons tended to fire/burst at the same moment (or within a close interval of each other), thereby generating a stronger response in HVC_{INT}^{10} . Therefore, the characteristic tonic activity that HVC interneurons exhibit with bursting and suppression at different locations during singing is explained in our model by the excitatory and inhibitory coupling between the interneurons and both classes of projecting neurons.

The inhibitory effect of HVCINT neurons, their interplay with the excitatory projection neurons, and their intrinsic properties plays a key role in the modulation of sequence propagation and overall desired network behavior. In particular, if the excitation from the projection neurons onto the interneurons was very large (>> gAMPA), then HVCINT neurons enter regimes of very dense and continuous bursting/spiking (above their natural and basic, yet already enhanced

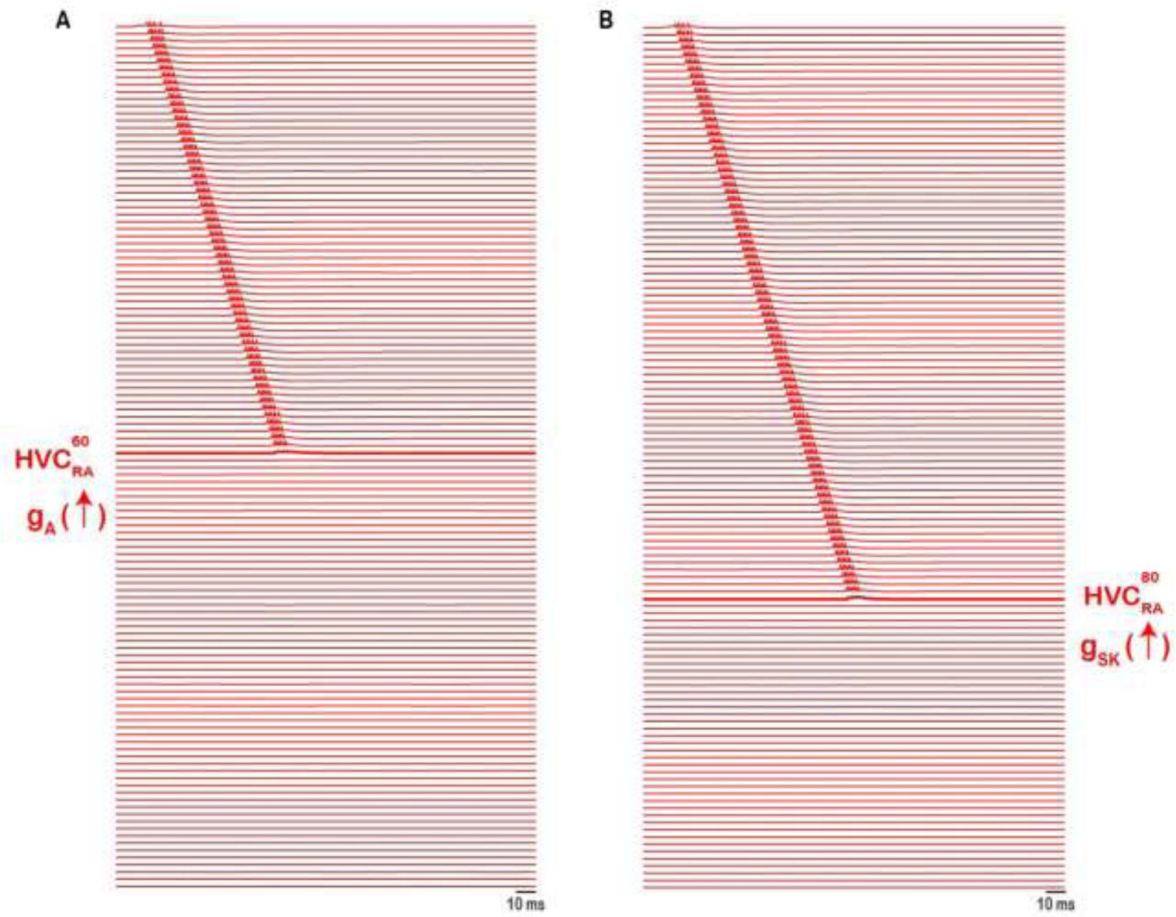

Figure 7.

Intrinsic changes in HVC_{RA} halts the propagation of sequential activity.

Up-regulating the A-type K^+ current (**A**) or the Ca^{2+} – dependent K^+ current (**B**) in exemplar neurons (HVC_{RA}^{60} , **A**) or (HVC_{RA}^{80} , **B**), by increasing g_A 10-fold (**A**), or g_{SK} from 15-fold nS (**B**), reduces the excitability of corresponding HVC_{RA} neuron markedly, eliminating its corresponding burst and breaking the sequence.

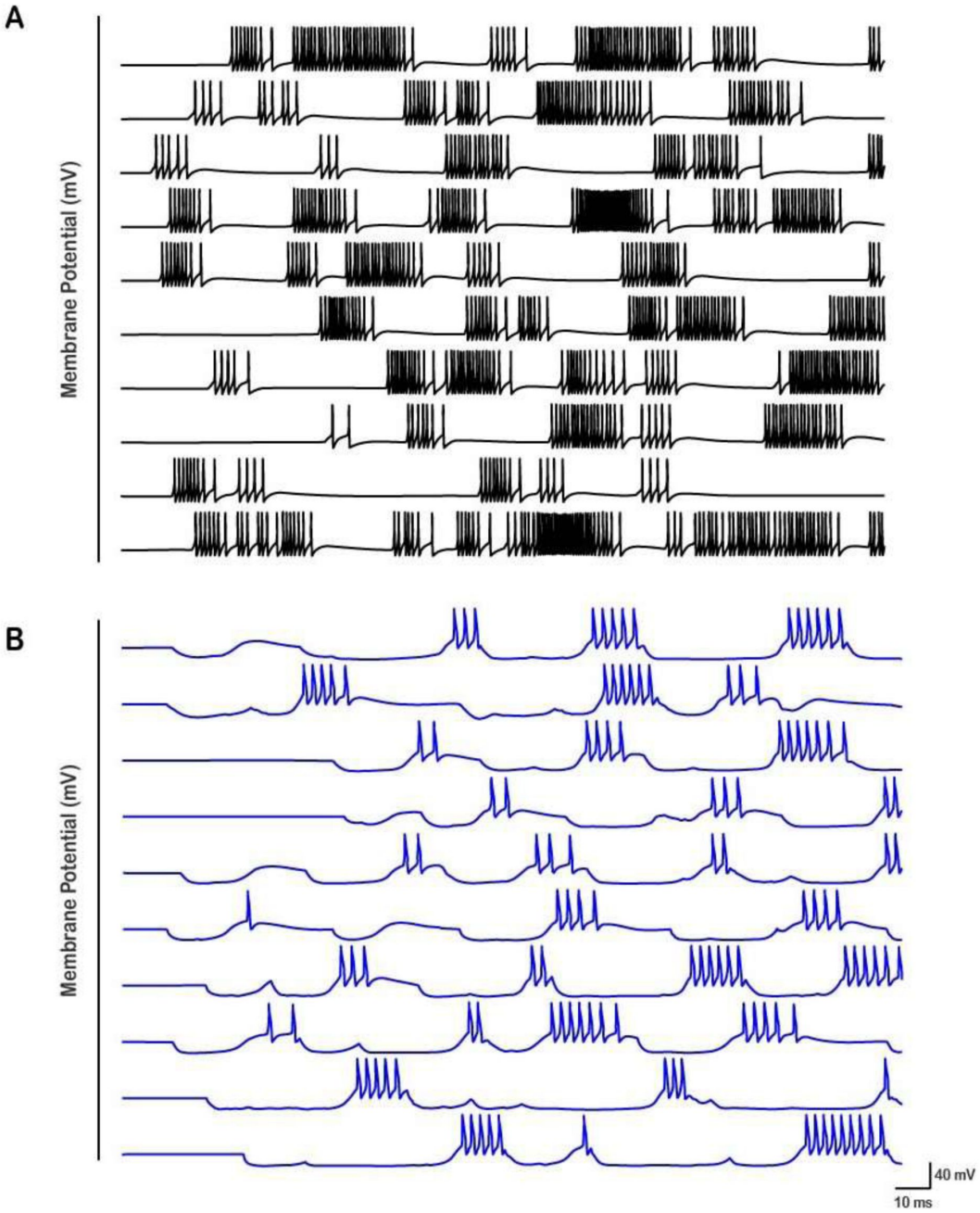

Figure 8.

Activity patterns for 10 HVC_{INT} and 10 HVC_X neurons are illustrated.

A. HVC interneurons displays dense spiking and bursting throughout the song, due to the dense HVC_{RA} – HVC_{INT} and HVC_X – HVC_{INT} excitatory coupling (**Fig. 4**). **B**. HVC_X neurons display 2-4 rebound bursts that vary in their strength and duration due to HVC_{INT} – HVC_X inhibitory coupling as well as intrinsic properties (**Fig. 9**).

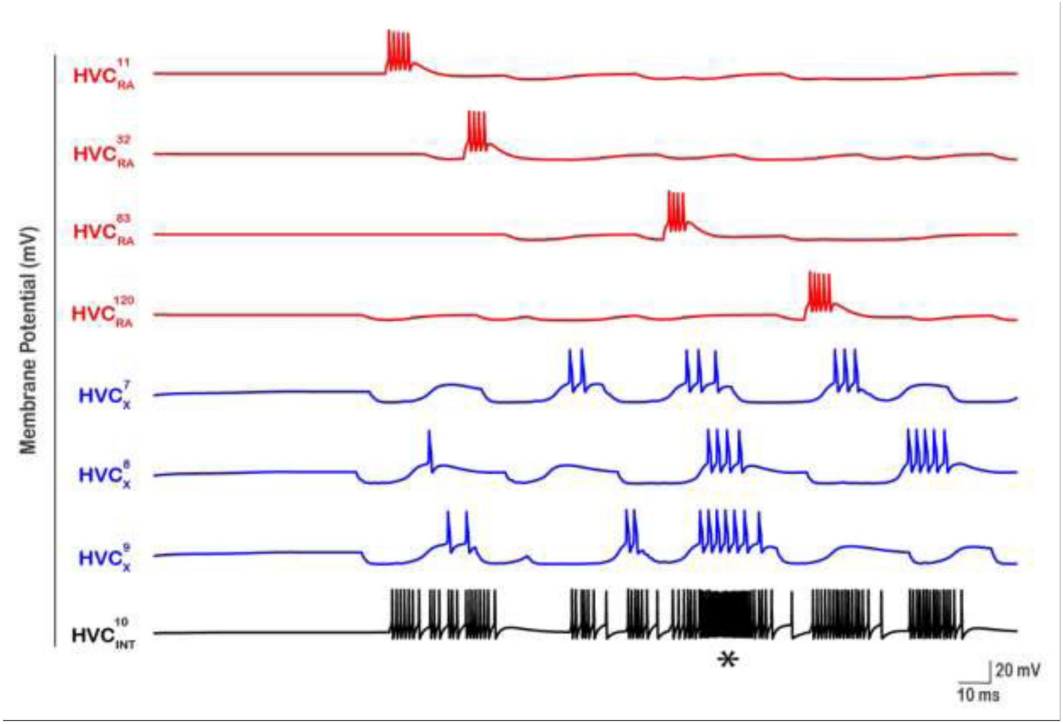

Figure 9.

Patterned activity of HVC interneurons illustrated for an exemplar interneuron (HVC_{INT}^{10}).

For this neuron, HVC_{RA}^{11}, HVC_{RA}^{32}, HVC_{RA}^{83}, HVC_{RA}^{120}, HVC_{X}^{7}, HVC_{X}^{8} and HVC_{X}^{9} were selected randomly from the pool of HVC_{RA}'s and HVC_X's to form excitatory coupling. The number of bursts in HVC_{INT}^{10} is controlled by the number of bursts that each of the HVC_{RA} and HVC_X neurons that connect to it exhibit. The strength of each of the HVC_{INT}^{10} bursts depend on the magnitude of g_{AMPA} from the corresponding neuron(s) they cause it as well as the simultaneous bursting of any of the projecting neurons. For example, the asterisk (*) shows a region of dense firing in HVC_{INT}^{10} because HVC_{RA}^{83}, HVC_{X}^{7}, HVC_{X}^{8} and HVC_{X}^{9} neurons elicit their spikes at similar times causing a potentiated response in HVC_{INT}^{10}. HVC_X neurons exhibit multiple sags and rebounds because they're receiving inhibition from several interneurons (not shown here).

potentiation), thereby leading to the inhibition of the HVCRA's, halting the sequence. Similarly, if the GABAergic conductances from HVCINT to HVCRA was relatively strong, outside their ideal ranges (**Figure 2-B**), then HVCRA neurons won't be able to elicit their bursts.

Besides the synaptic modulations of HVCINT neurons on network activity, intrinsic mechanisms orchestrated primarily by the T-type Ca^{2+} current and the hyperpolarization-activated inward current need to be tightly regulated to ensure desired network activity. The T-type calcium channel opens near resting membrane potential and markedly influence neuronal excitability (Huguenard, 1996; Jagodic et al., 2008). In our model, if the T-type Ca^{2+} current in an HVCINT neuron is up-regulated (due to a depolarizing shift in its voltage-dependent inactivation or simply setting g_{CaT} to a relatively large value), then the interneuron will fire with much larger firing frequency, silencing the corresponding HVCRA and HVCX neurons that it connects to and breaking the sequence (**Fig. 10A**). Similarly, the H-channels regulate the resting membrane potentials of the neurons they're expressed in and play a key role in regulating the spontaneous firing activity (Datunashvili et al., 2018; Funahashi et al., 2003; Yao et al., 2003). In our model, if the H conductance of an HVCINT was upregulated (by increasing the magnitude of gh), then the neuron switches to continuous firing, silencing the HVCRA's that is connects to (**Fig. 10B**). Therefore, both the interplay between excitation and inhibition between HVCINT and HVC projection neurons as well as the intrinsic properties of HVCINT neurons (ICaT and IH) are necessary elements to ensure an accurate propagation of sequential activity.

Rebound bursting in HVCX

The activity patterns that HVCX neurons exhibit in the network are illustrated in **Figure 8B** (shown here for 10 HVCX neurons). The X-projecting neuronal firing is characterized by regions of inhibition throughout singing, interrupted by occasional rebound bursting. The strength of each burst and the number of total bursts in an HVCX depend on synaptic and intrinsic mechanisms summarized briefly as such: 1) the degree of inhibition from HVCINT neurons, 2) the number and timing of bursts of HVCINT neurons and 3) the intrinsic properties and magnitudes of the T – type Ca^{2+} and H – currents that the HVCX neurons exhibit. In short, the stronger the GABAergic maximal conductance(s) from the HVCINT neurons that inhibit a given HVCX neuron, the stronger the HVCX neuron's rebound burst (**Figures 8**-**11**). Similarly, if multiple HVCINT neurons' bursts that inhibit an HVCX neuron aligned simultaneously, then the rebound in HVCX is potentiated due to the stronger inhibition. This is primarily due to the T-type Ca^{2+} current and the H-current that HVCX neurons exhibit, facilitating rapid calcium influx into the neurons when they rebound from hyperpolarization. The calcium influx is correlated to the degree and the duration of inhibition that the neuron receives, and can trigger a potentiated burst of action potentials leading to more robust rebound responses. In other words, the stronger the inhibition of HVCX, the stronger the activation of ICaT and Ih, leading to stronger rebounds. Moreover, the number of spikes in each HVCX burst is controlled by several factors including 1) the degree of inhibition from HVCINT and its effect on ICaT and Ih as described earlier, and 2) the strength of the Ca^{2+}-dependent K^+ conductance (g_{SK}) with stronger magnitudes of this conductance dampening the excitability of these neurons and reducing the number of spikes.

The interplay between HVCINT and HVCX in shaping the characteristic HVCX responses is illustrated in **Figure 11** from exemplar neurons in the network. Two interneurons, HVC^5_{INT} (black) and HVC^6_{INT} (green) were selected randomly to inhibit HVC^3_X (blue trace, **Fig. 11A**). There are several regions in the HVC^3_X membrane potential trajectory where the neuron is inhibited (sags/sinks in the voltage trace). These regions correspond to the moments in time when either HVC^5_{INT} or HVC^6_{INT} neurons, or both simultaneously, are bursting, thereby silencing HVC^3_X. Eventually, HVC^3_X is able to escape inhibition at a few instances in time and generate multiple post inhibitory rebound bursts mediated by I_{CaT} and I_h. **Figure 11B** shows a zoomed version of panel A illustrating the three rebound bursts in HVC^1_X as a result of escape from inhibition. HVC^5_{INT} and

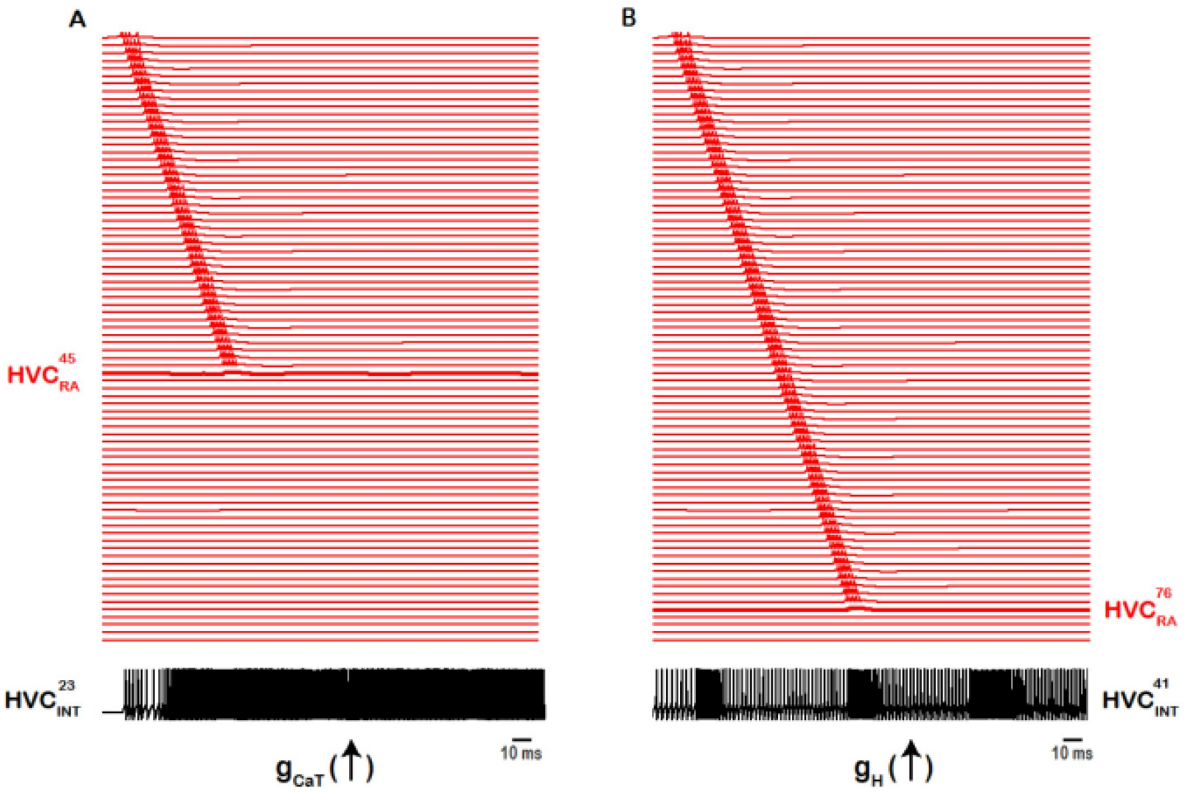

Figure 10.

Intrinsic changes in HVC_{INT} halts the propagation of sequential activity.

Up-regulating the T-type Ca^{2+} current conductance (**A**) or the hyperpolarization-activated inward current conductance (**B**) in exemplar HVC_{INT} neurons eliminates sequence propagation. Increasing g_{CaT} in HVC^{23}_{INT} HVC^{23} 10-fold results in dense bursting and firing in HVC^{23}_{INT}, which in its turn blocks the bursting of HVC^{45}_{RA} due to the inhibitory GABA coupling between HVC^{23}_{INT} and HVC^{45}_{RA} (**A**). Similarly, increasing g_H in HVC^{41}_{INT} 10-fold results in increased firing in HVC^{41}_{INT}, which in its turn blocks the bursting of HVC^{76}_{RA} due to the inhibitory GABA coupling between HVC^{41}_{INT} and HVC^{76}_{RA} (**B**). Sequence of HVC_{RA} bursts truncated at the level of HVC^{80}_{RA} for better visualization purposes.

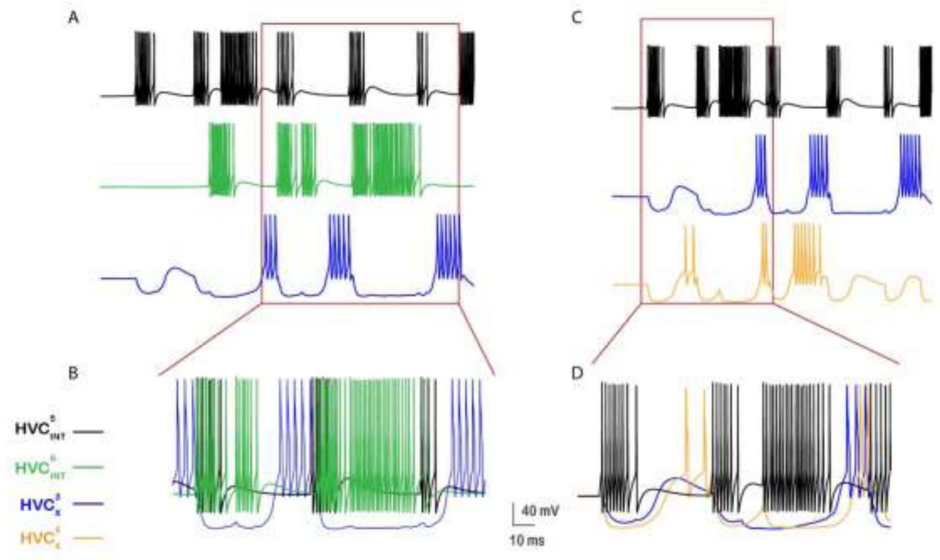

Figure 11.

Activity patterns illustrating the interplay between HVC interneurons and X-projecting neurons. HVC_X^3 **(blue) is an exemplar projecting neuron that receives inhibition from** HVC_{INT}^5 **(black) and** HVC_{INT}^6 **(green) due to the random inhibitory coupling**

(**A**). HVC_X^3 is inhibited whenever HVC_{INT}^5 and HVC_{INT}^6 are firing, eventually escaping inhibition at some intervals and eliciting rebound bursts due to the activation of I_H and I_{CaT}. HVC interneurons can inhibit multiple HVC_X neurons. HVC_{INT}^5 is an exemplar from the network that inhibits HVC_X^3 and HVC_Y^5 (orange) (**C**). Bursts in HVC_{INT}^5 elicit subsequent bursts in HVC_X^3 and HVC_Y^5 unless silenced by other HVC_{INT} neurons that connect to them. Zoomed versions of (**A**) and (**C**) are show in (**B**) and (**D**).

HVC^{6}_{INT} neurons generated multiple successive bursts of firing, during which HVC^{3}_{X} cannot escape the inhibition. There are only a few intervals where HVC^{3}_{X} is able to elicit rebound bursts; the first opportunity was at the beginning of the trace (**Fig. 11A**) where the sag generated in HVC^{3}_{X} as a result of inhibition from HVC^{5}_{INT} is clear, but the inhibition from HVC^{5}_{INT} was not strong enough to elicit a rebound burst in HVC^{3}_{X}, rather eliciting only a rebound depolarization. The subsequent three opportunities where HVC^{3}_{X} is able to escape the inhibition all elicited rebound bursts due to the strong inhibitory input arriving from both interneurons.

All rebound bursts in HVCX are orchestrated by the hyperpolarization-activated inward current (I_H) and the T-type Ca^{2+} current (I_{CaT}). The longer the duration of the inhibition prior to a rebound, the longer the time I_H and I_{CaT} take to fully activate and generate the rebound burst. The shorter the inhibitory silent interval (that is, the interval in which HVCX is receiving no inhibition), the shorter the rebound and the fewer the number of spikes in the rebound burst (**Fig. 11A**, first rebound burst). Moreover, HVC interneurons inhibit multiple HVCX neurons in our network. **Figure 11C** shows an exemplar interneuron (HVC^{5}_{INT}, black) that happens to inhibit two X-projecting neurons (HVC^{3}_{X}, blue and HVC^{5}_{INT}, orange). Each burst in HVC^{5}_{INT} elicits an iPSP in HVC^{3}_{X} and HVC^{5}_{INT}, and can contribute to subsequent rebound bursts in them unless silenced by other interneurons that connect to HVC^{3}_{X} or HVC^{5}_{INT} (**Fig. 11D**). All HVCX neurons differed in their corresponding number of rebound bursts as well as in the number of spikes per burst rendering the results biologically accurate.

As mentioned earlier, the T-type Ca^{2+} and the H-conductances play a significant role in modulating the rebound bursting in HVCX neurons. As a matter of fact, these two conductances, along with the Ca^{2+} – dependent K^{+} conductance can halt the sequential propagation of activity and mess up the overall desired network behavior as described next. Ramping up gH in HVCX neurons to values outside the allowed ranges (**Figure 2-A**) will break the sequence of propagation and generate nonrealistic firing patterns. The g_H parameter was increased in **Figure 12A** in an exemplar HVCX neuron (HVC^{36}_{X}) to large values, driving HVC^{36}_{X} into regimes of runaway excitation due to the up-regulation of I_H and generating a non-realistic firing pattern for a typical X-projecting neuron during singing. The reason the sequential propagation of HVCRA is halted is because HVC^{36}_{X} happens to have an excitatory coupling with HVC^{34}_{INT} (along with other interneurons, but we illustrate it here for HVC^{34}_{INT}), and as a result of HVC^{36}_{X}'s increased firing, HVC^{34}_{INT} generates a mostly-continuous firing trace of bursting and spiking, which silences the HVCRA neuron that it happens to inhibit (in this case, HVC^{70}_{RA}, **Fig. 12A**).

Similarly, altering gCaT in HVCX neurons can have similar effects on network activity. **Figure 12B** shows an exemplar HVCX neuron (HVC^{12}_{X}) where gCaT was ramped up to large values and as a result, stronger rebound bursts in HVC^{12}_{X} were elicited as well as larger number of rebound spikes in each burst. This is primarily due to the up-regulation of the T-type Ca^{2+} current that was induced, markedly influencing the neuronal excitability. The stronger rebounding in HVC^{12}_{X} generated stronger excitation in their postsynaptic interneurons' counterparts that they excite (for example, HVC^{16}_{INT}), which in their turn silenced the HVCRA neurons that they inhibit (for example, HVC^{80}_{RA} is the first neuron in the chain that HVC^{16}_{INT} inhibits, breaking the sequence at HVC^{80}_{RA}). And finally, the Ca^{2+} – dependent K^{+} conductance, which plays a key role in governing HVCX neurons' excitability and their characteristic spike frequency adaptation (Daou et al., 2013) can have similar effects if the channel was down-regulated (rather than up-regulated as in I_{CaT} and I). **Figure 12C** shows the effects of blocking the g_{SK} conductance in an exemplar HVCX neuron (HVC^{27}_{X}) leading to its increased firing, which in turn leads to stronger bursting and spiking in the HVCINT neurons it excites (for example, HVC^{30}_{INT}). HVC^{30}_{INT} in its turn generates stronger and wider-range inhibition onto the HVCRA neurons it sends its axons to (for example, HVC^{15}_{RA} is the first neuron in the chain HVC^{30}_{INT} inhibits, silencing it and breaking the sequence at HVC^{15}_{RA}).

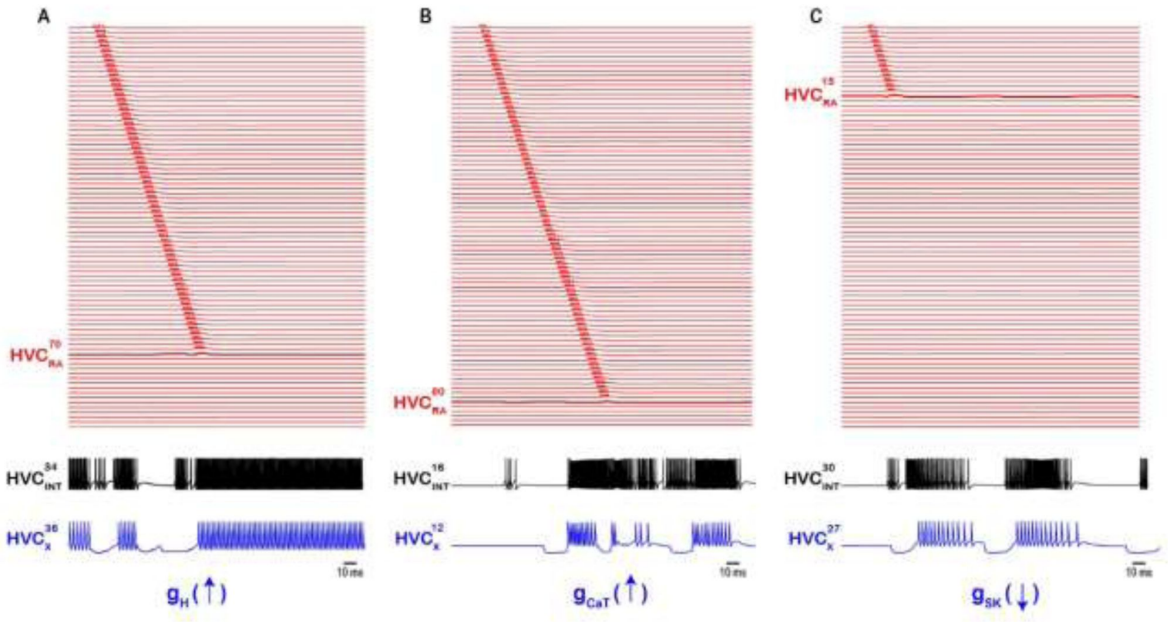

Figure 12.

Intrinsic changes in HVC_X halts the propagation of sequential activity.

A. Up-regulating the hyperpolarization-activated inward current conductance in a sample HVC_X neuron (HVC_x^{36} , by increasing its *g* 10-fold) leads to increased firing in all HVC_{INT} neurons it connects to (for example, HVC_{INT}^{34}), which in its turn inhibits all HVC_{RA} neurons it connects to (for example, HVC_{RA}^{70} , being first in the pool that it inhibits) breaking the sequence at the level of HVC_{RA}^{70} . **B**. Up-regulating the T-type Ca^{2+} current conductance in a sample HVC_X neuron (HVC_x^{12} , by increasing its *gCaT* 15-fold) leads to stronger rebound bursts in HVC_x^{12} which leads to increased firing in all HVC_{INT} neurons it connects to (for example, HVC_{INT}^{16}), which in its turn inhibits all HVC_{RA} neurons it connects to (for example, HVC_{RA}^{80} , being first in the pool that it inhibits) breaking the sequence at the level of HVC_{RA}^{80} . **C**. Finally, down-regulating the Ca^{2+} – dependent K^+ current conductance in a sample HVC_X neuron (HVC_x^{27} , by setting its g_{SK} to zero) leads to stronger rebound bursts in HVC_x^{27} which leads to increased firing in all HVC_{INT} neurons it connects to (for example, HVC_{INT}^{30}), which in its turn inhibits all HVC_{RA} neurons it connects to (for example, HVC_{RA}^{15} , being first in the pool that it inhibits) breaking the sequence at the level of HVC_{RA}^{15} . Sequence of HVC_{RA} bursts truncated at the level of HVC_{RA}^{85} for better visualization purposes.

Finally, we checked the consequences of altering the intrinsic properties of HVC_X neurons on the network's desired behavior. To do so, we varied the maximal conductances of the three principal ionic currents of the X-projecting neurons (I_{CaT}, I_{SK}, I_H) across all neurons of the population, while keeping this variation within the reported ranges shown in **Figure 2A** (because certainly going outside these ranges will disrupt network activity for other reasons as reported in **Figures 10** and **12**). Varying those three key paramters across the HVCx population had different results. In 100 different simulations that generated random maximal conductances for I_{CaT},I_{SK} and I_H, 41% of the simulations did not have any considerable effect on the desired network activity, whereas 59% resulted in disrupted network activity, and sometimes detrimental. For example, **Figure 13** shows an example where the sequential propagation of activity was halted and the firing patterns of some interneurons and X-projecting neurons were rendered non-biophysically realistic. Particularly, some interneurons switched to continuous spiking or phasic bursting with little episodic bursting modes, while some HVC_X neurons generated longer rebounds, fewer number of bursts or fewer number of spikes per burst (**Fig. 13** B-C). Hence, changes in the intrinsic properties of X-projecting neurons can disrupt activity propagation necessary for song production, and produce biologically unrealistic bursting patterns in HVC neurons. This can wreak havoc on our network model hinting to the finding that biophysical parameters are distinct and consistent for an individual bird and this unique combination is needed for song (Daou & Margoliash, 2020). The homogeneity in the intrinsic properties of X-projectors might be a strategy allowing it to adapt or respond to changes in the network.

In conclusion, we developed a detailed and biophysically realistic neural network model for sequence propagation in the HVC of the zebra finch. Our model consisted of chains of microcircuits, each comprised of a selection of HVCRA, HVCINT and HVCX model neurons selected randomly from a total pool of neurons. The maximal conductances of the four key and principle ionic currents for each model neuron, the number of neurons of each class in any microcircuit, and the excitatory and inhibitory connections between the different classes within a microcircuit and across microcircuits are all selected randomly. This activity propagates throughout the chain of microcircuits causing a sequence of HVCRA bursts while leaving behind realistic bursting patterns for all classes of HVC neurons as seen during singing. The model incorporates all known ionic and synaptic currents for each HVC neuron. The network architecture we developed was able to replicate the *in vivo* biologically realistic firing behavior for each class by including sparse timely-locked bursting in the RA-projecting neurons (with accurate intrinsic properties for each burst in terms of number of spikes, duration and spike morphology), multiple bursting in the X-projecting neurons that are also sparse and time-locked, and dense bursting/spiking in the interneurons with few intermittent quiescence. The ability of our network to reproduce the sequential propagation of activity in the presence of excitatory and inhibitory connections involving all neuronal subclasses as well as over a range of values for each synaptic and ionic maximal conductances is an indication of its robustness. Our network unveiled key intrinsic and synaptic mechanisms that modulate the sequential propagation of neural activity by highlighting important roles for the T-type Ca^{2+} current and hyperpolarization activated (H) inward current in HVCX and HVCINT neurons, Ca^{2+}-dependent K^+ current in HVCX and HVCRA, A-type K^+ current in HVCRA, as well as GABAergic and glutamatergic synaptic currents that connects all neuronal subclasses together. The result is an improved characterization of the HVC network responsible for song production in the zebra finch.

Discussion

In this study, we have designed a neural network model that describe zebra finch song production in the HVC. The biophysically realistic network architecture that we designed combine both classes of HVC projection neurons with local inhibitory interneurons. A fundamental goal that we have achieved in our design is a successful replication of the *in vivo* firing behaviors of all the HVC neuronal classes: single sparse timely-precise bursting (3-6 spikes for ~10 ms) in the RA-projecting

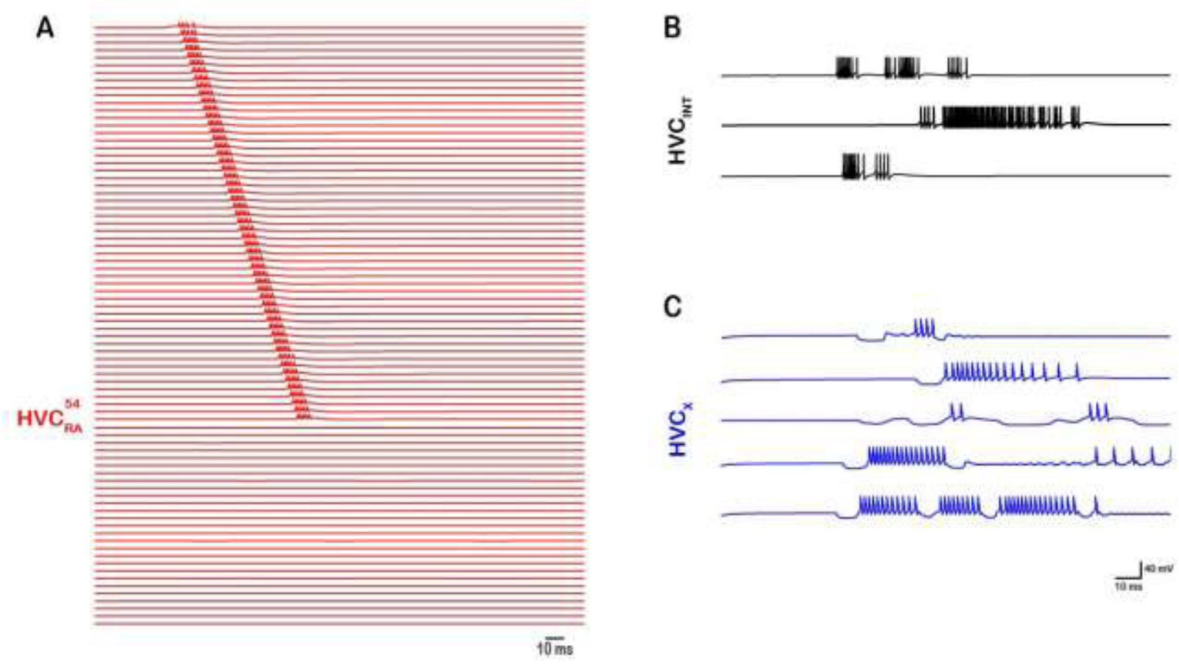

Figure 13.

Altering the intrinsic properties of HVCx neurons disrupt network activity in 59% of the cases (out of 100 simulations) where the maximal conductances (gCaT, gSK and gH) of HVCx neurons are randomly varied within their allowed ranges (Figure 2A).

As a result, some HVC interneurons (B) and X-projecting neurons (C) generated non-biological realistic firing patterns, halting the propagation of sequential activity in RA-projectors (A).

neurons, multiple bursting (1-4 bursts with 4-9 spikes/burst) in the X-projecting neurons, dense and frequent bursting in the interneurons, as well as the general intrinsic properties that each class of HVC neurons exhibit (Daou et al., 2013; Lewicki, 1996; Long et al., 2010). The patterning activity in HVC is largely shaped in our model by the intrinsic properties of the individual neurons as well as the synaptic properties where excitation and inhibition play a major role in enabling neurons to generate their characteristic bursts during singing.

The three classes of model neurons incorporated to our network as well as the synaptic currents that connect them are based on Hodgkin-Huxley formalisms that contain ion channels and synaptic currents which had been pharmacologically identified (Daou et al., 2013; Kosche et al., 2015; Mooney & Prather, 2005). Our network showed that sequence propagation can be broken if several intrinsic mechanisms are perturbed. In particular, if ICaT or IH are upregulated in HVCX or HVCINT, if ISK is downregulated in HVCX or if ISK is upregulated in HVCRA, then the corresponding chain of activity stops and the rhythmic activity of the network is disrupted (**Figures 7**, **10** and **12**). Synaptically, perhaps the most critical role in our network design is played by interneurons which orchestrate the activity of the two projection neurons in a structured manner. Interneurons adjust the timing of HVC projection neurons' bursts (Amador et al., 2013; Kosche et al., 2015), and developmental learning regulates inhibition onto HVCRA (Vallentin et al., 2016). HVCRA neurons interact with HVCX through local interneurons, a disynaptic inhibitory pathway that conveys information to HVCX neurons (Prather et al., 2008). Focal application of the GABAA receptor antagonist, gabazine, restricted inhibitory impact in HVC leading to stronger and faster responses relative to call onset (Benichov & Vallentin, 2020), showing that local HVC interneurons form an inhibitory mask that can greatly constrain the spiking activity of projecting neurons (Kornfeld et al., 2017; Kosche et al., 2015; Mooney & Prather, 2005) suggesting that HVC model networks that lack inhibitory neurons are inadequate for explaining sequential propagation of neural activity.

Various models of how the song is encoded within HVC have been proposed. Some groups suggested that bursting activity propagates through a chain of synaptically connected HVCRA neurons either as single neurons (Fee et al., 2004; Hahnloser et al., 2002; Long et al., 2010) or as pools of HVCRA neurons, each group driving a distinct ensemble of RA neurons (Jin et al., 2007; Leonardo & Fee, 2005; Li & Greenside, 2006). These models assume that HVCRA neurons generate a continuous, feed-forward sequence of activity over time, with little or no role played by X-projecting HVC neurons and interneurons. Other models have incorporated alternative temporal encoding mechanisms by necessitating synaptic integration at the levels of HVCRA and HVCINT populations (Drew & Abbott, 2003; Gibb et al., 2009a; Jin, 2009; Weber & Hahnloser, 2007) while yet other approaches gave emphasis to brainstem feedback processes by incorporating inter-hemispheric coordination to activate sequences of syllable-specific HVCRA and HVCINT neurons (Galvis et al., 2018; Gibb et al., 2009b). A prominent model used spatially recurrent excitatory chains and local feedback inhibition to show how the HVC network stabilize synchrony while propagating sequential activity (Cannon et al., 2015; Markowitz et al., 2015).

All existing models that describe premotor sequence generation in the HVC either assume a distributed model (Elmaleh et al., 2021) that dictates that local HVC circuitry is not sufficient to advance the sequence but rather depends upon moment-to-moment feedback through Uva (Hamaguchi et al., 2016), or assume models that rely on intrinsic connections within HVC to propagate sequential activity. In the latter case, some models assume that HVC is composed of multiple discrete subnetworks that encode individual song elements (Glaze & Troyer, 2013; Long & Fee, 2008; Wang et al., 2008), but lacks the local connectivity to link the subnetworks, while other models assume that HVC may have sufficient information in its intrinsic connections to form a single continuous network sequence (Long et al., 2010).

The network architecture we developed here exhibits overlap with the various models presented. First, in agreement with the continuous model, our network architecture displays a feed-forward mechanism regulating the circuit dynamics e.g., (Gibb et al., 2009a; Jin, 2009; Jin et al., 2007; Li & Greenside, 2006; Long et al., 2010). Nonetheless, diverging from a linear progression of HVC neurons directing the song, the network's structure comprises sequences of microcircuits incorporating all classes of HVC neurons, where sequential activity transmits from one microcircuit to the next, as opposed to transitioning directly between individual neurons. Second, in agreement with the subnetwork models, our model envisions HVC as comprised of multiple discrete subcircuits (SSSs) where each microcircuit incorporates its own pool of neurons; however, in our model HVC's connectivity is sufficient to link the microcircuits together and extrinsic influences are not needed. Moreover, our network is in agreement with the (Cannon et al., 2015) model where structured inhibition is needed to propagate sequential activity, synchronize the firing of pools of neurons and stabilize spike timing along the chain. The pivotal element in advancing sequential activity through time is the inhibition exerted by HVCINT onto HVCX and HVCRA neurons, facilitated in the case of HVCX through rebound firing, and all orchestrated by intrinsic mechanisms.

A potential drawback of our model is that it does not incorporate brainstem feedback processes or address inter-hemispheric coordination as proposed by others (Galvis et al., 2018; Gibb et al., 2009b). Another drawback is its sole focus on local excitatory connectivity within the HVC (Kornfeld et al., 2017; Long et al., 2010). Moreover, HVC neurons receive afferent excitatory connections (Akutagawa & Konishi, 2010; Nottebohm et al., 1982) that plays significant roles in their local dynamics. For example, the excitatory inputs that HVC neurons receive from Uvaeformis may be crucial in initiating (Andalman et al., 2011; Danish et al., 2017; Galvis et al., 2018) or sustaining (Hamaguchi et al., 2016) the sequential activity.

The role of ion channels in controlling network activity

Our model highlights the role of principal ion channels (IH, ICaT, ISK and IA) in controlling HVC's network dynamics and progressing its neural sequence. Hyperpolarization-activated ionic conductances had been widely observed across various electrically excitable cells (Pape, 1996) and play significant roles in rhythmogenesis (Budde et al., 1997; Golowasch et al., 1992; Golowasch & Marder, 1992). In our network, model HVCX neurons are not able to elicit their rebound bursting without I_H and sequence is halted if this conductance is upregulated in either of HVCX or HVCINT (**Figures 8-10**, 11 and 12). Similarly, the T-type Ca^{2+} current is recognized as crucial in various systems as an ionic contributor to burst generation (Deschenes et al., 1982; Fraser & MacVicar, 1991; Huguenard, 1996; Llinás & Yarom, 1981). Lewicki (1996) observed a significant hyperpolarization in some HVC neurons *in vivo* before they emit their corresponding bursts, and the intensity of the burst correlates with the degree of hyperpolarization. In this study, we have illustrated its pivotal role in rebound spiking where up-regulating this conductance in HVCX or HVCINT halts sequence propagation (**Figures 8-10**, 11 and 12). Moreover, the A-type K^+ current is involved in several rhythmogenic activities controlling membrane excitability (Coetzee et al., 1999; Ellis et al., 2007; Gross et al., 2016) and in our network, upregulating IA suppress bursting in model HVCRA and breaks sequence propagation (**Fig. 7**). Finally, the small conductance Ca^{2+}-activated potassium current (I_{SK}) plays important roles in the regulation of excitable cells controlling network rhythmic activity (Benítez et al., 2011; Chen et al., 2014; Pedarzani et al., 2005) and in our network I_{SK} plays a significant role since its upregulation in HVCRA or its downregulation in HVCX eliminates sequence propagation (**Fig.7** and **Fig. 12** respectively).

In conclusion, the network model developed provide a large step forward in describing the biophysics of HVC circuitry, and may throw a new light on certain dynamics in the mammalian brain, particularly the motor cortex (Shmiel et al., 2006) and the hippocampus regions (Lee & Wilson, 2002) where precisely-timed sequential activity is crucial. We suggest that temporally-precise sequential activity may be a manifestation of neural networks comprised of chain of

microcircuits, each containing pools of excitatory and inhibitory neurons, with local interplay among neurons of the same microcircuit and global interplays across the various microcircuits, and with structured inhibition and intrinsic properties synchronizing the neuronal pools and stabilizing timing within the ongoing sequence.

References

1. Akutagawa E., Konishi M 2010) **New brain pathways found in the vocal control system of a songbird** *Journal of Comparative Neurology* **518**:3086–3100

2. Amador A., Perl Y. S., Mindlin G. B., Margoliash D 2013) **Elemental gesture dynamics are encoded by song premotor cortical neurons** *Nature* **495**:59–64

3. Andalman A. S., Foerster J. N., Fee M. S 2011) **Control of vocal and respiratory patterns in birdsong: dissection of forebrain and brainstem mechanisms using temperature** *PLoS One* **6**:e25461

4. Benichov J. I., Vallentin D 2020) **Inhibition within a premotor circuit controls the timing of vocal turn-taking in zebra finches** *Nature communications* **11**:221

5. Benítez B. A., Belálcazar H. M., Anastasía A., Mamah D. T., Zorumski C. F., Mascó D. H., Herrera D. G., De Erausquin G. A. 2011) **Functional reduction of SK3-mediated currents precedes AMPA-receptor-mediated excitotoxicity in dopaminergic neurons** *Neuropharmacology* **60**:1176–1186

6. Budde T., Biella G., Munsch T., Pape H. C 1997) **Lack of Regulation by Intracellular Ca2+ of the Hyper Polarization-Activated Cation Current in Rat Thalamic Neurones** *The Journal of physiology* **503**:79–85

7. Cannon J., Kopell N., Gardner T., Markowitz J 2015) **Neural sequence generation using spatiotemporal patterns of inhibition** *PLoS computational biology* **11**:e1004581

8. Chen L., Deltheil T., Turle-Lorenzo N., Liberge M., Rosier C., Watabe I., Sreng L., Amalric M., Mourre C 2014) **SK channel blockade reverses cognitive and motor deficits induced by nigrostriatal dopamine lesions in rats** *International Journal of Neuropsychopharmacology* **17**:1295–1306

9. Coetzee W. A., Amarillo Y., Chiu J., Chow A., Lau D., McCormack T., Morena H., Nadal M. S., Ozaita A., Pountney D 1999) **Molecular diversity of K+ channels** *Annals of the New York Academy of Sciences* **868**:233–255

10. Danish H. H., Aronov D., Fee M. S 2017) **Rhythmic syllable-related activity in a songbird motor thalamic nucleus necessary for learned vocalizations** *PLoS One* **12**:e0169568

11. Daou A., Margoliash D 2020) **Intrinsic neuronal properties represent song and error in zebra finch vocal learning** *Nature communications* **11**:952

12. Daou A., Ross M. T., Johnson F., Hyson R. L., Bertram R 2013) **Electrophysiological characterization and computational models of HVC neurons in the zebra finch** *Journal of neurophysiology* **110**:1227–1245

13. Datunashvili M., Chaudhary R., Zobeiri M., Lüttjohann A., Mergia E., Baumann A., Balfanz S., Budde B., Van Luijtelaar G., Pape H.-C. 2018) **Modulation of hyperpolarization-activated inward current and thalamic activity modes by different cyclic nucleotides** *Frontiers in cellular neuroscience* **12**:369

14. Deschenes M., Roy J., Steriade M 1982) **Thalamic bursting mechanism: an inward slow current revealed by membrane hyperpolarization** *Brain research* **239**:289–293

15. Destexhe A., Babloyantz A 1993) **A model of the inward current Ih and its possible role in thalamocortical oscillations** *Neuroreport* **4**:223–226

16. Destexhe A., Mainen Z. F., Sejnowski T. J 1994) **Synthesis of models for excitable membranes, synaptic transmission and neuromodulation using a common kinetic formalism** *Journal of computational neuroscience* **1**:195–230

17. Drew P. J., Abbott L 2003) **Model of song selectivity and sequence generation in area HVc of the songbird** *Journal of neurophysiology* **89**:2697–2706

18. Dunmyre J. R., Del Negro C. A., Rubin J. E 2011) **Interactions of persistent sodium and calcium-activated nonspecific cationic currents yield dynamically distinct bursting regimes in a model of respiratory neurons** *Journal of computational neuroscience* **31**:305–328

19. Dutar P., Vu H. M., Perkel D. J 1998) **Multiple cell types distinguished by physiological, pharmacological, and anatomic properties in nucleus HVc of the adult zebra finch** *Journal of neurophysiology* **80**:1828–1838

20. Egger R., Tupikov Y., Elmaleh M., Katlowitz K. A., Benezra S. E., Picardo M. A., Moll F., Kornfeld J., Jin D. Z., Long M. A 2020) **Local axonal conduction shapes the spatiotemporal properties of neural sequences** *Cell* **183**:537–548

21. Ellis L. D., Krahe R. d., Bourque C. W., Dunn R. J., Chacron M. J. 2007) **Muscarinic receptors control frequency tuning through the downregulation of an A-type potassium current** *Journal of neurophysiology* **98**:1526–1537

22. Elmaleh M., Kranz D., Asensio A. C., Moll F. W., Long M. A 2021) **Sleep replay reveals premotor circuit structure for a skilled behavior** *Neuron* **109**:3851–3861

23. Fee M. S., Goldberg J. H 2011) **A hypothesis for basal ganglia-dependent reinforcement learning in the songbird** *Neuroscience* **198**:152–170

24. Fee M. S., Kozhevnikov A. A., Hahnloser R. H 2004) **Neural mechanisms of vocal sequence generation in the songbird** *Annals of the New York Academy of Sciences* **1016**:153–170

25. Fee M. S., Scharff C 2010) **The songbird as a model for the generation and learning of complex sequential behaviors** *ILAR journal* **51**:362–377

26. Fraser D. D., MacVicar B. A 1991) **Low-threshold transient calcium current in rat hippocampal lacunosum-moleculare interneurons: kinetics and modulation by neurotransmitters** *Journal of Neuroscience* **11**:2812–2820

27. Fujimoto H., Hasegawa T., Watanabe D 2011) **Neural coding of syntactic structure in learned vocalizations in the songbird** *Journal of Neuroscience* **31**:10023–10033

28. Funahashi M., Mitoh Y., Kohjitani A., Matsuo R 2003) **Role of the hyperpolarization-activated cation current (Ih) in pacemaker activity in area postrema neurons of rat brain slices** *The Journal of physiology* **552**:135–148

29. Galvis D., Wu W., Hyson R. L., Johnson F., Bertram R 2018) **Interhemispheric dominance switching in a neural network model for birdsong** *Journal of neurophysiology* **120**:1186–1197

30. Gibb L., Gentner T. Q., Abarbanel H. D 2009a) **Brain stem feedback in a computational model of birdsong sequencing** *Journal of neurophysiology* **102**:1763–1778

31. Gibb L., Gentner T. Q., Abarbanel H. D 2009b) **Inhibition and recurrent excitation in a computational model of sparse bursting in song nucleus HVC** *Journal of neurophysiology* **102**:1748–1762

32. Glaze C. M., Troyer T. W 2013) **Development of temporal structure in zebra finch song** *Journal of neurophysiology* **109**:1025–1035

33. Golowasch J., Buchholtz F., Epstein I. R., Marder E 1992) **Contribution of individual ionic currents to activity of a model stomatogastric ganglion neuron** *Journal of neurophysiology* **67**:341–349

34. Golowasch J., Casey M., Abbott L., Marder E 1999) **Network stability from activity-dependent regulation of neuronal conductances** *Neural computation* **11**:1079–1096

35. Golowasch J., Marder E 1992) **Ionic currents of the lateral pyloric neuron of the stomatogastric ganglion of the crab** *Journal of neurophysiology* **67**:318–331

36. Gross C., Yao X., Engel T., Tiwari D., Xing L., Rowley S., Danielson S. W., Thomas K. T., Jimenez-Mateos E. M., Schroeder L. M 2016) **MicroRNA-mediated downregulation of the potassium channel Kv4. 2 contributes to seizure onset** *Cell reports* **17**:37–45

37. Hahnloser R. H., Kozhevnikov A. A., Fee M. S 2002) **An ultra-sparse code underliesthe generation of neural sequences in a songbird** *Nature* **419**:65–70

38. Hamaguchi K., Tanaka M., Mooney R 2016) **A distributed recurrent network contributes to temporally precise vocalizations** *Neuron* **91**:680–693

39. Harvey C. D., Coen P., Tank D. W 2012) **Choice-specific sequences in parietal cortex during a virtual-navigation decision task** *Nature* **484**:62–68

40. Hodgkin A. L., Huxley A. F 1952) **A quantitative description of membrane current and its application to conduction and excitation in nerve** *The Journal of physiology* **117**:500

41. Huguenard J 1996) **Low-threshold calcium currents in central nervous system neurons** *Annual review of physiology* **58**:329–348

42. Jagodic M. M., Pathirathna S., Joksovic P. M., Lee W., Nelson M. T., Naik A. K., Su P., Jevtovic-Todorovic V., Todorovic S. M 2008) **Upregulation of the T-type calcium current in small rat sensory neurons after chronic constrictive injury of the sciatic nerve** *Journal of neurophysiology* **99**:3151–3156

43. Jin D. Z 2009) **Generating variable birdsong syllable sequences with branching chain networks in avian premotor nucleus HVC** *Physical Review E* **80**:051902

44. Jin D. Z., Ramazanoğlu F. M., Seung H. S 2007) **Intrinsic bursting enhances the robustness of a neural network model of sequence generation by avian brain area HVC** *Journal of computational neuroscience* **23**:283–299

45. Kornfeld J., Benezra S. E., Narayanan R. T., Svara F., Egger R., Oberlaender M., Denk W., Long M. A 2017) **EM connectomics reveals axonal target variation in a sequence-generating network** *eLife* **6**:e24364

46. Kosche G., Vallentin D., Long M. A 2015) **Interplay of inhibition and excitation shapes a premotor neural sequence** *Journal of Neuroscience* **35**:1217–1227

47. Kozhevnikov A. A., Fee M. S 2007) **Singing-related activity of identified HVC neurons in the zebra finch** *Journal of neurophysiology* **97**:4271–4283

48. Kubota M., Saito N 1991) **Sodium-and calcium-dependent conductances of neurones in the zebra finch hyperstriatum ventrale pars caudale in vitro** *The Journal of physiology* **440**:131–142

49. Kubota M., Taniguchi I 1998) **Electrophysiological characteristics of classes of neuron in the HVc of the zebra finch** *Journal of neurophysiology* **80**:914–923

50. Lee A. K., Wilson M. A 2002) **Memory of sequential experience in the hippocampus during slow wave sleep** *Neuron* **36**:1183–1194

51. Leonardo A., Fee M. S 2005) **Ensemble coding of vocal control in birdsong** *Journal of Neuroscience* **25**:652–661

52. Lewicki M. S 1996) **Intracellular characterization of song-specific neurons in the zebra finch auditory forebrain** *Journal of Neuroscience* **16**:5854–5863

53. Li M., Greenside H 2006) **Stable propagation of a burst through a one-dimensional homogeneous excitatory chain model of songbird nucleus HVC** *Physical Review E* **74**:011918

54. Llinás R., Yarom Y 1981) **Properties and distribution of ionic conductances generating electroresponsiveness of mammalian inferior olivary neurones in vitro** *The Journal of physiology* **315**:569–584

55. Long M. A., Fee M. S 2008) **Using temperature to analyse temporal dynamics in the songbird motor pathway** *Nature* **456**:189–194

56. Long M. A., Jin D. Z., Fee M. S 2010) **Support for a synaptic chain model of neuronal sequence generation** *Nature* **468**:394–399

57. MacDonald C. J., Lepage K. Q., Eden U. T., Eichenbaum H 2011) **Hippocampal "time cells" bridge the gap in memory for discontiguous events** *Neuron* **71**:737–749

58. Marder E., Goaillard J.-M 2006) **Variability, compensation and homeostasis in neuron and network function** *Nature Reviews Neuroscience* **7**:563–574

59. Markowitz J. E., Liberti W. A., Guitchounts G., Velho T., Lois C., Gardner T. J 2015) **Mesoscopic patterns of neural activity support songbird cortical sequences** *PLoS biology* **13**:e1002158

60. Mooney R 2000) **Different subthreshold mechanisms underlie song selectivity in identified HVc neurons of the zebra finch** *Journal of Neuroscience* **20**:5420–5436

61. Mooney R 2009) **Neurobiology of song learning** *Current opinion in neurobiology* **19**:654–660

62. Mooney R., Hoese W., Nowicki S 2001) **Auditory representation of the vocal repertoire in a songbird with multiple song types** *Proceedings of the national academy of sciences* **98**:12778–12783

63. Mooney R., Prather J. F 2005) **The HVC microcircuit: the synaptic basis for interactions between song motor and vocal plasticity pathways** *Journal of Neuroscience* **25**:1952–1964

64. Nottebohm F., Paton J. A., Kelley D. B 1982) **Connections of vocal control nuclei in the canary telencephalon** *Journal of Comparative Neurology* **207**:344–357

65. Pape H.-C 1996) **Queer current and pacemaker: the hyperpolarization-activated cation current in neurons** *Annual review of physiology* **58**:299–327

66. Pastalkova E., Itskov V., Amarasingham A., Buzsaki G 2008) **Internally generated cell assembly sequences in the rat hippocampus** *Science* **321**:1322–1327

67. Pedarzani P., McCutcheon J. E., Rogge G., Jensen B. S., Christophersen P., Hougaard C., Strøbæk D., Stocker M 2005) **Specific enhancement of SK channel activity selectively potentiates the afterhyperpolarizing current IAHP and modulates the firing properties of hippocampal pyramidal neurons** *Journal of Biological Chemistry* **280**:41404–41411

68. Peters A. J., Chen S. X., Komiyama T 2014) **Emergence of reproducible spatiotemporal activity during motor learning** *Nature* **510**:263–267

69. Prather J. F., Peters S., Nowicki S., Mooney R 2008) **Precise auditory–vocal mirroring in neurons for learned vocal communication** *Nature* **451**:305–310

70. Roberts T. F., Hisey E., Tanaka M., Kearney M. G., Chattree G., Yang C. F., Shah N. M., Mooney R 2017) **Identification of a motor-to-auditory pathway important for vocal learning** *Nature neuroscience* **20**:978–986

71. Schmitt L. I., Wimmer R. D., Nakajima M., Happ M., Mofakham S., Halassa M. M 2017) **Thalamic amplification of cortical connectivity sustains attentional control** *Nature* **545**:219–223

72. Shea S. D., Koch H., Baleckaitis D., Ramirez J.-M., Margoliash D 2010) **Neuron-specific cholinergic modulation of a forebrain song control nucleus** *Journal of neurophysiology* **103**:733–745

73. Shmiel T., Drori R., Shmiel O., Ben-Shaul Y., Nadasdy Z., Shemesh M., Teicher M, Abeles M. 2006) **Temporally precise cortical firing patterns are associated with distinct action segments** *Journal of neurophysiology* **96**:2645–2652

74. Skaggs W. E., McNaughton B. L., Wilson M. A., Barnes C. A 1996) **Theta phase precession in hippocampal neuronal populations and the compression of temporal sequences** *Hippocampus* **6**:149–172

75. Terman D., Rubin J. E., Yew A., Wilson C 2002) **Activity patterns in a model for the subthalamopallidal network of the basal ganglia** *Journal of Neuroscience* **22**:2963–2976

76. Vallentin D., Kosche G., Lipkind D., Long M. A 2016) **Inhibition protects acquired song segments during vocal learning in zebra finches** *Science* **351**:267–271

77. Varela J. A., Sen K., Gibson J., Fost J., Abbott L., Nelson S. B 1997) **A quantitative description of short-term plasticity at excitatory synapses in layer 2/3 of rat primary visual cortex** *Journal of Neuroscience* **17**:7926–7940

78. Wang C. Z. H., Herbst J. A., Keller G. B., Hahnloser R. H. R 2008) **Rapid interhemispheric switching during vocal production in a songbird** *PLoS biology* **6**:e250

79. Wang P., Liu H., Wang L., Gao R. X 2018) **Deep learning-based human motion recognition for predictive context-aware human-robot collaboration** *CIRP annals* **67**:17–20

80. Wang X.-J., Liu Y., Sanchez-Vives M. V., McCormick D. A 2003) **Adaptation and temporal decorrelation by single neurons in the primary visual cortex** *Journal of neurophysiology* **89**:3279–3293

81. Weber A. P., Hahnloser R. H. R 2007) **Spike correlations in a songbird agree with a simple Markov population model** *PLoS computational biology* **3**:e249

82. Wild J. M., Williams M. N., Howie G. J., Mooney R 2005) **Calcium-binding proteins define interneurons in HVC of the zebra finch (Taeniopygia guttata)** *Journal of Comparative Neurology* **483**:76–90

83. Williams A. H., O'Leary T., Marder E. 2013) **Homeostatic regulation of neuronal excitability** *Scholarpedia* **8**:1656

84. Yao H., Donnelly D. F., Ma C., LaMotte R. H 2003) **Upregulation of the hyperpolarization-activated cation current after chronic compression of the dorsal root ganglion** *Journal of Neuroscience* **23**:2069–2074

85. Yu A. C., Margoliash D 1996) **Temporal hierarchical control of singing in birds** *Science* **273**:1871–1875

Author information

Zeina Bou Diab
Biomedical Engineering Program, American University of Beirut, Beirut, Lebanon

Marc Chammas
Biomedical Engineering Program, American University of Beirut, Beirut, Lebanon

Arij Daou
Biomedical Engineering Program, American University of Beirut, Beirut, Lebanon
ORCID iD: 0000-0001-7590-4774

For correspondence: arij.daou@aub.edu.lb

Editors

Reviewing Editor
Jesse Goldberg
Cornell University, Ithaca, United States of America

Senior Editor
Andrew King
University of Oxford, Oxford, United Kingdom

Reviewer #1 (Public review):

Summary:

The paper presents a model for sequence generation in the zebra finch HVC, which adheres to cellular properties measured experimentally. However, the model is fine-tuned and exhibits limited robustness to noise inherent in the inhibitory interneurons within the HVC, as well as to fluctuations in connectivity between neurons. Although the proposed microcircuits are introduced as units for sub-syllabic segments (SSS), the backbone of the network remains a feedforward chain of HVC_RA neurons, similar to previous models.

Strengths:

The model incorporates all three of the major types of HVC neurons. The ion channels used and their kinetics are based on experimental measurements. The connection patterns of the neurons are also constrained by the experiments.

Weaknesses:

The model is described as consisting of micro-circuits corresponding to SSS. This presentation gives the impression that the model's structure is distinct from previous models, which connected HVC_RA neurons in feedforward chain networks (Jin et al 2007, Li & Greenside, 2006; Long et al 2010; Egger et al 2020). However, the authors implement single HVC_RA neurons into chain networks within each micro-circuit and then connect the end of the chain to the start of the chain in the subsequent micro-circuit. Thus, the HVC_RA neuron in their model forms a single-neuron chain. This structure is essentially a simplified version of earlier models.

In the model of the paper, the chain network drives the HVC_I and HVC_X neurons. The role of the micro-circuits is more significant in organizing the connections: specifically, from HVC_RA neurons to HVC_I neurons, and from HVC_I neurons to both HVC_X and HVC_RA neurons.

How useful is this concept of micro-circuits? HVC neurons fire continuously even during the silent gaps. There are no SSS during these silent gaps.

A significant issue of the current model is that the HVC_RA to HVC_RA connections require fine-tuning, with the network functioning only within a narrow range of g_AMPA (Figure 2B). Similarly, the connections from HVC_I neurons to HVC_RA neurons also require fine-tuning. This sensitivity arises because the somatic properties of HVC_RA neurons are insufficient to produce the stereotypical bursts of spikes observed in recordings from singing birds, as demonstrated in previous studies (Jin et al 2007; Long et al 2010). In these previous works, to address this limitation, a dendritic spike mechanism was introduced to generate an intrinsic bursting capability, which is absent in the somatic compartment of HVC_RA neurons. This dendritic mechanism significantly enhances the robustness of the chain network, eliminating the need to fine-tune any synaptic conductances, including those from HVC_I neurons (Long et al 2010).

Why is it important that the model should NOT be sensitive to the connection strengths?

First, the firing of HVC_I neurons is highly noisy and unreliable. HVC_I neurons fire spontaneous, random spikes under baseline conditions. During singing, their spike timing is imprecise and can vary significantly from trial to trial, with spikes appearing or disappearing across different trials. As a result, their inputs to HVC_RA neurons are inherently noisy. If the model relies on precisely tuned inputs from HVC_I neurons, the natural fluctuations in HVC_I firing would render the model non-functional. The authors should incorporate noisy HVC_I

neurons into their model to evaluate whether this noise would render the model non-functional.

Second, Kosche et al. (2015) demonstrated that reducing inhibition by suppressing HVC_I neuron activity makes HVC_RA firing less sparse but does not compromise the temporal precision of the bursts. In this experiment, the local application of gabazine should have severely disrupted HVC_I activity. However, it did not affect the timing precision of HVC_RA neuron firing, emphasizing the robustness of the HVC timing circuit. This robustness is inconsistent with the predictions of the current model, which depends on finely tuned inputs and should, therefore, be vulnerable to such disruptions.

Third, the reliance on fine-tuning of HVC_RA connections becomes problematic if the model is scaled up to include groups of HVC_RA neurons forming a chain network, rather than the single HVC_RA neurons used in the current work. With groups of HVC_RA neurons, the summation of presynaptic inputs to each HVC_RA neuron would need to be precisely maintained for the model to function. However, experimental evidence shows that the HVC circuit remains functional despite perturbations, such as a few degrees of cooling, micro-lesions, or turnover of HVC_RA neurons. Such robustness cannot be accounted for by a model that depends on finely tuned connections, as seen in the current implementation.

The authors examined how altering the channel properties of neurons affects the activity in their model. While this approach is valid, many of the observed effects may stem from the delicate balancing required in their model for proper function.

In the current model, HVC_X neurons burst as a result of rebound activity driven by the I_H current. Rebound bursts mediated by the I_H current typically require a highly hyperpolarized membrane potential. However, this mechanism would fail if the reversal potential of inhibition is higher than the required level of hyperpolarization. Furthermore, Mooney (2000) demonstrated that depolarizing the membrane potential of HVC_X neurons did not prevent bursts of these neurons during forward playback of the bird's own song, suggesting that these bursts (at least under anesthesia, which may be a different state altogether) are not necessarily caused by rebound activity. This discrepancy should be addressed or considered in the model.

Some figures contain direct copies of figures from published papers. It is perhaps a better practice to replace them with schematics if possible.

https://doi.org/10.7554/eLife.105526.1.sa1

Reviewer #2 (Public review):

Summary:

In this paper, the authors use numerical simulations to try to understand better a major experimental discovery in songbird neuroscience from 2002 by Richard Hahnloser and collaborators. The 2002 paper found that a certain class of projection neurons in the premotor nucleus HVC of adult male zebra finch songbirds, the neurons that project to another premotor nucleus RA, fired sparsely (once per song motif) and precisely (to about 1 ms accuracy) during singing.

The experimental discovery is important to understand since it initially suggested that the sparsely firing RA-projecting neurons acted as a simple clock that was localized to HVC and that controlled all details of the temporal hierarchy of singing: notes, syllables, gaps, and motifs. Later experiments suggested that the initial interpretation might be incomplete: that the temporal structure of adult male zebra finch songs instead emerged in a more complicated and distributed way, still not well understood, from the interaction of HVC with

multiple other nuclei, including auditory and brainstem areas. So at least two major questions remain unanswered more than two decades after the 2002 experiment: What is the neurobiological mechanism that produces the sparse precise bursting: is it a local circuit in HVC or is it some combination of external input to HVC and local circuitry? And how is the sparse precise bursting in HVC related to a songbird's vocalizations?

The authors only investigate part of the first question, whether the mechanism for sparse precise bursts is local to HVC. They do so indirectly, by using conductance-based Hodgkin-Huxley-like equations to simulate the spiking dynamics of a simplified network that includes three known major classes of HVC neurons and such that all neurons within a class are assumed to be identical. A strength of the calculations is that the authors include known biophysically deduced details of the different conductances of the three major classes of HVC neurons, and they take into account what is known, based on sparse paired recordings in slices, about how the three classes connect to one another. One weakness of the paper is that the authors make arbitrary and not well-motivated assumptions about the network geometry, and they do not use the flexibility of their simulations to study how their results depend on their network assumptions. A second weakness is that they ignore many known experimental details such as projections into HVC from other nuclei, dendritic computations (the somas and dendrites are treated by the authors as point-like isopotential objects), the role of neuromodulators, and known heterogeneity of the interneurons. These weaknesses make it difficult for readers to know the relevance of the simulations for experiments and for advancing theoretical understanding.

Strengths:

The authors use conductance-based Hodgkin-Huxley-like equations to simulate spiking activity in a network of neurons intended to model more accurately songbird nucleus HVC of adult male zebra finches. Spiking models are much closer to experiments than models based on firing rates or on 2-state neurons.

The authors include information deduced from modeling experimental current-clamp data such as the types and properties of conductances. They also take into account how neurons in one class connect to neurons in other classes via excitatory or inhibitory synapses, based on sparse paired recordings in slices by other researchers.

The authors obtain some new results of modest interest such as how changes in the maximum conductances of four key channels (e.g., A-type K+ currents or Ca-dependent K+ currents) influence the structure and propagation of bursts, while simultaneously being able to mimic accurately current-clamp voltage measurements.

Weaknesses:

One weakness of this paper is the lack of a clearly stated, interesting, and relevant scientific question to try to answer. In the introduction, the authors do not discuss adequately which questions recent experimental and theoretical work have failed to explain adequately, concerning HVC neural dynamics and its role in producing vocalizations. The authors do not discuss adequately why they chose the approach of their paper and how their results address some of these questions.

For example, the authors need to explain in more detail how their calculations relate to the works of Daou et al, J. Neurophys. 2013 (which already fitted spiking models to neuronal data and identified certain conductances), to Jin et al J. Comput. Neurosci. 2007 (which already discussed how to get bursts using some experimental details), and to the rather similar paper by E. Armstrong and H. Abarbanel, J. Neurophys 2016, which already postulated and studied sequences of microcircuits in HVC. This last paper is not even cited by the authors.

The authors' main achievement is to show that simulations of a certain simplified and idealized network of spiking neurons, which includes some experimental details but ignores many others, match some experimental results like current-clamp-derived voltage time series for the three classes of HVC neurons (although this was already reported in earlier work by Daou and collaborators in 2013), and simultaneously the robust propagation of bursts with properties similar to those observed in experiments. The authors also present results about how certain neuronal details and burst propagation change when certain key maximum conductances are varied.

However, these are weak conclusions for two reasons. First, the authors did not do enough calculations to allow the reader to understand how many parameters were needed to obtain these fits and whether simpler circuits, say with fewer parameters and simpler network topology, could do just as well. Second, many previous researchers have demonstrated robust burst propagation in a variety of feed-forward models. So what is new and important about the authors' results compared to the previous computational papers?

Also missing is a discussion, or at least an acknowledgment, of the fact that not all of the fine experimental details of undershoots, latencies, spike structure, spike accommodation, etc may be relevant for understanding vocalization. While it is nice to know that some models can match these experimental details and produce realistic bursts, that does not mean that all of these details are relevant for the function of producing precise vocalizations. Scientific insights in biology often require exploring which of the many observed details can be ignored and especially identifying the few that are essential for answering some questions. As one example, if HVC-X neurons are completely removed from the authors' model, does one still get robust and reasonable burst propagation of HVC-RA neurons? While part of the nucleus HVC acts as a premotor circuit that drives the nucleus RA, part of HVC is also related to learning. It is not clear that HVC-X neurons, which carry out some unknown calculation and transmit information to area X in a learning pathway, are relevant for burst production and propagation of HVC-RA neurons, and so relevant for vocalization. Simulations provide a convenient and direct way to explore questions of this kind.

One key question to answer is whether the bursting of HVC-RA projection neurons is based on a mechanism local to HVC or is some combination of external driving (say from auditory nuclei) and local circuitry. The authors do not contribute to answering this question because they ignore external driving and assume that the mechanism is some kind of intrinsic feed-forward circuit, which they put in by hand in a rather arbitrary and poorly justified way, by assuming the existence of small microcircuits consisting of a few HVC-RA, HVC-X, and HVC-I neurons that somehow correspond to "sub-syllabic segments". To my knowledge, experiments do not suggest the existence of such microcircuits nor does theory suggest the need for such microcircuits.

Another weakness of this paper is an unsatisfactory discussion of how the model was obtained, validated, and simulated. The authors should state as clearly as possible, in one location such as an appendix, what is the total number of independent parameters for the entire network and how parameter values were deduced from data or assigned by hand. With enough parameters and variables, many details can be fit arbitrarily accurately so researchers have to be careful to avoid overfitting. If parameter values were obtained by fitting to data, the authors should state clearly what the fitting algorithm was (some iterative nonlinear method, whose results can depend on the initial choice of parameters), what the error function used for fitting (sum of least squares?) was, and what data were used for the fitting.

The authors should also state clearly the dynamical state of the network, the vector of quantities that evolve over time. (What is the dimension of that vector, which is also the number of ordinary differential equations that have to be integrated?) The authors do not

mention what initial state was used to start the numerical integrations, whether transient dynamics were observed and what were their properties, or how the results depended on the choice of the initial state. The authors do not discuss how they determined that their model was programmed correctly (it is difficult to avoid typing errors when writing several pages or more of a code in any language) or how they determined the accuracy of the numerical integration method beyond fitting to experimental data, say by varying the time step size over some range or by comparing two different integration algorithms.

Also disappointing is that the authors do not make any predictions to test, except rather weak ones such as that varying a maximum conductance sufficiently (which might be possible by using dynamic clamps) might cause burst propagation to stop or change its properties. Based on their results, the authors do not make suggestions for further experiments or calculations, but they should.

https://doi.org/10.7554/eLife.105526.1.sa0

Author response:

> ***eLife Assessment***
>
> *Birdsong production depends on precise neural sequences in a vocal motor nucleus HVC. In this useful biophysical model, Daou and colleagues identify specific biophysical parameters that result in sparse neural sequences observed in vivo. While the model is presently incomplete because it is overfit to produce sequences and therefore not robust to real biological variation, the model has the potential to address some outstanding issues in HVC function.*

We are grateful for the extensive supportive comments from the reviewers, including broad, strong appreciation of the novel aspects of our manuscript. We believe these will be only strengthened in the next submission.

> ***Public Reviews:***
>
> ***Reviewer #1 (Public review):***
>
> *Summary:*
>
> *The paper presents a model for sequence generation in the zebra finch HVC, which adheres to cellular properties measured experimentally. However, the model is fine-tuned and exhibits limited robustness to noise inherent in the inhibitory interneurons within the HVC, as well as to fluctuations in connectivity between neurons. Although the proposed microcircuits are introduced as units for sub-syllabic segments (SSS), the backbone of the network remains a feedforward chain of HVC_RA neurons, similar to previous models.*
>
> *Strengths:*
>
> *The model incorporates all three of the major types of HVC neurons. The ion channels used and their kinetics are based on experimental measurements. The connection patterns of the neurons are also constrained by the experiments.*
>
> *Weaknesses:*
>
> *The model is described as consisting of micro-circuits corresponding to SSS. This presentation gives the impression that the model's structure is distinct from previous models, which connected HVC_RA neurons in feedforward chain networks (Jin et al 2007,*

> *Li & Greenside, 2006; Long et al 2010; Egger et al 2020). However, the authors implement single HVC_RA neurons into chain networks within each micro-circuit and then connect the end of the chain to the start of the chain in the subsequent micro-circuit. Thus, the HVC_RA neuron in their model forms a single-neuron chain. This structure is essentially a simplified version of earlier models.*
>
> *In the model of the paper, the chain network drives the HVC_I and HVC_X neurons. The role of the micro-circuits is more significant in organizing the connections: specifically, from HVC_RA neurons to HVC_I neurons, and from HVC_I neurons to both HVC_X and HVC_RA neurons.*

We thank Reviewer 1 for their thoughtful comments.

While the reviewer is correct about the fact that the propagation of sequential activity in this model is primarily carried by HVC_{RA} neurons in a feed-forward manner, we need to emphasize that this is true only if there is no intrinsic or synaptic perturbation to the HVC network. For example, we showed in Figures 10 and 12 how altering the intrinsic properties of HVC_X neurons or for interneurons disrupts sequence propagation. In other words, while HVC_{RA} neurons are the key forces to carry the chain forward, the interplay between excitation and inhibition in our network as well as the intrinsic parameters for all classes of HVC neurons are equally important forces in carrying the chain of activity forward. Thus, the stability of activity propagation necessary for song production depend on a finely balanced network of HVC neurons, with all classes contributing to the overall dynamics. Moreover, all existing models that describe premotor sequence generation in the HVC either assume a distributed model (Elmaleh et al., 2021) that dictates that local HVC circuitry is not sufficient to advance the sequence but rather depends upon momentto-moment feedback through Uva (Hamaguchi et al., 2016), or assume models that rely on intrinsic connections within HVC to propagate sequential activity. In the latter case, some models assume that HVC is composed of multiple discrete subnetworks that encode individual song elements (Glaze & Troyer, 2013; Long & Fee, 2008; Wang et al., 2008), but lacks the local connectivity to link the subnetworks, while other models assume that HVC may have sufficient information in its intrinsic connections to form a single continuous network sequence (Long et al. 2010). The HVC model we present extends the concept of a feedforward network by incorporating additional neuronal classes that influence the propagation of activity (interneurons and HVC_X neurons). We have shown that any disturbance of the intrinsic or synaptic conductances of these latter neurons will disrupt activity in the circuit even when HVC_{RA} neurons properties are maintained.

In regard to the similarities between our model and earlier models, several aspects of our model distinguish it from prior work. In short, while several models of how sequence is generated within HVC have been proposed (Cannon et al., 2015; Drew & Abbott, 2003; Egger et al., 2020; Elmaleh et al., 2021; Galvis et al., 2018; Gibb et al., 2009a, 2009b; Hamaguchi et al., 2016; Jin, 2009; Long & Fee, 2008; Markowitz et al., 2015), all the models proposed either rely on intrinsic HVC circuitry to propagate sequential activity, rely on extrinsic feedback to advance the sequence or rely on both. These models do not capture the complex details of spike morphology, do not include the right ionic currents, do not incorporate all classes of HVC neurons, or do not generate realistic firing patterns as seen in vivo. Our model is the first biophysically realistic model that incorporates all classes of HVC neurons and their intrinsic properties. We tuned the intrinsic and the synaptic properties bases on the traces collected by Daou et al. (2013) and Mooney and Prather (2005) as shown in Figure 3. The three classes of model neurons incorporated to our network as well as the synaptic currents that connect them are based on HodgkinHuxley formalisms that contain ion channels and synaptic currents which had been pharmacologically identified. This is an advancement over prior models that primarily focused on the role of synaptic interactions or external inputs. The model is based on a feedforward chain of microcircuits that encode for the different sub-

syllabic segments and that interact with each other through structured feedback inhibition, defining an ordered sequence of cell firing. Moreover, while several models highlight the critical role of inhibitory interneurons in shaping the timing and propagation of bursts of activity in HVC_{RA} neurons, our work offers an intricate and comprehensive model that help understand this critical role played by inhibition in shaping song dynamics and ensuring sequence propagation.

> *How useful is this concept of micro-circuits? HVC neurons fire continuously even during the silent gaps. There are no SSS during these silent gaps.*

Regarding the concern about the usefulness of the 'microcircuit' concept in our study, we appreciate the comment and we are glad to clarify its relevance in our network. While we acknowledge that HVC_{RA} neurons interconnect microcircuits, our model's dynamics are still best described within the framework of microcircuitry particularly due to the firing behavior of HVC_X neurons and interneurons. Here, we are referring to microcircuits in a more functional sense, rather than rigid, isolated spatial divisions (Cannon et al. 2015). A microcircuit in our model reflects the local rules that govern the interaction between all HVC neuron classes within the broader network, and that are essential for proper activity propagation. For example, HVC_{INT} neurons belonging to any microcircuit burst densely and at times other than the moments when the corresponding encoded SSS is being “sung”. What makes a particular interneuron belong to this microcircuit or the other is merely the fact that it cannot inhibit HVC_{RA} neurons that are housed in the microcircuit it belongs to. In particular, if HVC_{INT} inhibits HVC_{RA} in the same microcircuit, some of the HVC_{RA} bursts in the microcircuit might be silenced by the dense and strong HVC_{INT} inhibition breaking the chain of activity again. Similarly, HVC_X neurons were selected to be housed within microcircuits due to the following reason: if an HVC_X neuron belonging to microcircuit *i* sends excitatory input to an HVC_{INT} neuron in microcircuit *j*, and that interneuron happens to select an HVC_{RA} neuron from microcircuit *i*, then the propagation of sequential activity will halt, and we’ll be in a scenario similar to what was described earlier for HVC_{INT} neurons inhibiting HVC_{RA} neurons in the same microcircuit.

We agree that there are no sub-syllabic segments described during the silent gaps and we thank the reviewer to pointing this out. Although silent gaps are integral to the overall process of song production, we have not elaborated on them in this model due to the lack of a clear, biophysically grounded representation for the gaps themselves at the level of HVC. Our primary focus has been on modeling the active, syllable-producing phases of the song, where the HVC network’s sequential dynamics are critical for song. However, one can think the encoding of silent gaps via similar mechanisms that encode SSSs, where each gap is encoded by similar microcircuits comprised of the three classes of HVC neurons (let’s called them GAP rather than SSS) that are active only during the silent gaps. In this case, the propagation of sequential activity is carried throughout the GAPs from the last SSS of the previous syllable to the first SSS of the subsequent syllable. We’ll make sure to emphasize this mechanism more in the revised version of the manuscript.

> *A significant issue of the current model is that the HVC_RA to HVC_RA connections require fine-tuning, with the network functioning only within a narrow range of g_AMPA (Figure 2B). Similarly, the connections from HVC_I neurons to HVC_RA neurons also require fine-tuning. This sensitivity arises because the somatic properties of HVC_RA neurons are insufficient to produce the stereotypical bursts of spikes observed in recordings from singing birds, as demonstrated in previous studies (Jin et al 2007; Long et al 2010). In these previous works, to address this limitation, a dendritic spike mechanism was introduced to generate an intrinsic bursting capability, which is absent in the somatic compartment of HVC_RA neurons. This dendritic mechanism significantly enhances the*

> *robustness of the chain network, eliminating the need to fine-tune any synaptic conductances, including those from HVC_I neurons (Long et al 2010).*
>
> *Why is it important that the model should NOT be sensitive to the connection strengths?*

We thank the reviewer for the comment. While mathematical models designed for highly complex nonlinear biological processes tangentially touch the biological realism, the current network as is right now is the first biologically realistic-enough network model designed for HVC that explains sequence propagation. We do not include dendritic processes in our network although that increases the realistic dynamics for various reasons. 1) The ion channels we integrated into the somatic compartment are known pharmacologically (Daou et al. 2013), but we don't know about the dendritic compartment's intrinsic properties of HVC neurons and the cocktail of ion channels that are expressed there. 2) We are able to generate realistic bursting in HVC_{RA} neurons despite the single compartment, and the main emphasis in this network is on the interactions between excitation and inhibition, the effects of ion channels in modulating sequence propagation, etc. 3) The network model already incorporates thousands of ODEs that govern the dynamics of each of the HVC neurons, so we did not want to add more complexity to the network especially that we don't know the biophysical properties of the dendritic compartments.

Therefore, our present focus is on somatic dynamics and the interaction between HVC_{RA} and HVC_{INT} neurons, but we acknowledge the importance of these processes in enhancing network resiliency. Although we agree that adding dendritic processes improves robustness, we still think that somatic processes alone can offer insightful information on the sequential dynamics of the HVC network. While the network should be robust across a wide range of parameters, it is also essential that certain parameters are designed to filter out weaker signals, ensuring that only reliable, precise patterns of activity propagate. Hence, we specifically chose to make the HVC_{RA}-to-HVC_{RA} excitatory connections more sensitive (narrow range of values) such that only strong, precise and meaningful stimuli can propagate through the network representing the high stereotypy and precision seen in song production.

> *First, the firing of HVC_I neurons is highly noisy and unreliable. HVC_I neurons fire spontaneous, random spikes under baseline conditions. During singing, their spike timing is imprecise and can vary significantly from trial to trial, with spikes appearing or disappearing across different trials. As a result, their inputs to HVC_RA neurons are inherently noisy. If the model relies on precisely tuned inputs from HVC_I neurons, the natural fluctuations in HVC_I firing would render the model non-functional. The authors should incorporate noisy HVC_I neurons into their model to evaluate whether this noise would render the model non-functional.*

We acknowledge that under baseline and singing settings, interneurons fire in an extremely noisy and inaccurate manner, although they exhibit time locked episodes in their activity (Hahnloser et al 2002, Kozhinikov and Fee 2007). In order to mimic the biological variability of these neurons, our model does, in fact, include a stochastic current to reflect the intrinsic noise and random variations in interneuron firing shown *in vivo* (and we highlight this in the Methods). If necessary and to make sure the network is resilient to this randomness in interneuron firing, we will investigate different approaches to enhance the noise representation even further and check its effect on sequence propagation.

> *Second, Kosche et al. (2015) demonstrated that reducing inhibition by suppressing HVC_I neuron activity makes HVC_RA firing less sparse but does not compromise the temporal precision of the bursts. In this experiment, the local application of gabazine should have severely disrupted HVC_I activity. However, it did not affect the timing precision of HVC_RA neuron firing, emphasizing the robustness of the HVC timing circuit. This*

> *robustness is inconsistent with the predictions of the current model, which depends on finely tuned inputs and should, therefore, be vulnerable to such disruptions.*

We thank the reviewer for the comment. The differences between the Kosche et al. (2015**)** findings and the predictions of our model arise from differences in the aspect of HVC function we are modeling. Our model is more sensitive to inhibition, which is a designed mechanism for achieving precise song patterning. This is a modeling simplification we adopted to capture specific characteristics of HVC function. Hence, Kosche et al. (2015) findings do not invalidate the approach of our model, but highlights that HVC likely operates with several**,** redundant mechanisms that overall ensure temporal precision**.** Nevertheless, we will investigate further the effects of the degree of inhibition on song patterning.

> *Third, the reliance on fine-tuning of HVC_RA connections becomes problematic if the model is scaled up to include groups of HVC_RA neurons forming a chain network, rather than the single HVC_RA neurons used in the current work. With groups of HVC_RA neurons, the summation of presynaptic inputs to each HVC_RA neuron would need to be precisely maintained for the model to function. However, experimental evidence shows that the HVC circuit remains functional despite perturbations, such as a few degrees of cooling, micro-lesions, or turnover of HVC_RA neurons. Such robustness cannot be accounted for by a model that depends on finely tuned connections, as seen in the current implementation.*

Our model of individual HVC_{RA} neurons and as stated previously is reductive model that focuses on understanding the mechanisms that govern sequential neural activity. We agree that scaling the model to include many of HVC_{RA} neurons poses challenges, specifically concerning the summation of presynaptic inputs. However, our model can still be adapted to a larger network without requiring the level of fine-tuning currently needed. In fact, the current fine-tuning of synaptic connections in the model is a reflection of fundamental network mechanisms rather than a limitation when scaling to a larger network. Besides, one important feature of this neural network is redundancy. Even if some neurons or synaptic connections are impaired, other neurons or pathways can compensate for these changes, allowing the activity propagation to remain intact.

> *The authors examined how altering the channel properties of neurons affects the activity in their model. While this approach is valid, many of the observed effects may stem from the delicate balancing required in their model for proper function.*
>
> *In the current model, HVC_X neurons burst as a result of rebound activity driven by the I_H current. Rebound bursts mediated by the I_H current typically require a highly hyperpolarized membrane potential. However, this mechanism would fail if the reversal potential of inhibition is higher than the required level of hyperpolarization. Furthermore, Mooney (2000) demonstrated that depolarizing the membrane potential of HVC_X neurons did not prevent bursts of these neurons during forward playback of the bird's own song, suggesting that these bursts (at least under anesthesia, which may be a different state altogether) are not necessarily caused by rebound activity. This discrepancy should be addressed or considered in the model.*

In our HVC network model, one goal with HVC_X neurons is to generate bursts in their underlying neuron population. Since HVC_X neurons in our model receive only inhibitory inputs from interneurons, we rely on inhibition followed by rebound bursts orchestrated by the IH and the I_{CaT} currents to achieve this goal. The interplay between the T-type Ca^{++} current and the H current in our model is fundamental to generate their corresponding bursts, as they are sufficient for producing the desired behavior in the network. Due to this interplay, we do not need significant inhibition to generate rebound bursts, because the T-

type Ca^{++} current's conductance can be stronger leading to robust rebound bursting even when the degree of inhibition is not very strong. We will highlight this with more clarity in the revised version.

> *Some figures contain direct copies of figures from published papers. It is perhaps a better practice to replace them with schematics if possible.*

We will replace the relevant figures with schematic representations where possible.

> ***Reviewer #2 (Public review):***
>
> *Summary:*
>
> *In this paper, the authors use numerical simulations to try to understand better a major experimental discovery in songbird neuroscience from 2002 by Richard Hahnloser and collaborators. The 2002 paper found that a certain class of projection neurons in the premotor nucleus HVC of adult male zebra finch songbirds, the neurons that project to another premotor nucleus RA, fired sparsely (once per song motif) and precisely (to about 1 ms accuracy) during singing.*
>
> *The experimental discovery is important to understand since it initially suggested that the sparsely firing RA-projecting neurons acted as a simple clock that was localized to HVC and that controlled all details of the temporal hierarchy of singing: notes, syllables, gaps, and motifs. Later experiments suggested that the initial interpretation might be incomplete: that the temporal structure of adult male zebra finch songs instead emerged in a more complicated and distributed way, still not well understood, from the interaction of HVC with multiple other nuclei, including auditory and brainstem areas. So at least two major questions remain unanswered more than two decades after the 2002 experiment: What is the neurobiological mechanism that produces the sparse precise bursting: is it a local circuit in HVC or is it some combination of external input to HVC and local circuitry?*
>
> *And how is the sparse precise bursting in HVC related to a songbird's vocalizations?*
>
> *The authors only investigate part of the first question, whether the mechanism for sparse precise bursts is local to HVC. They do so indirectly, by using conductance-based Hodgkin-Huxley-like equations to simulate the spiking dynamics of a simplified network that includes three known major classes of HVC neurons and such that all neurons within a class are assumed to be identical. A strength of the calculations is that the authors include known biophysically deduced details of the different conductances of the three major classes of HVC neurons, and they take into account what is known, based on sparse paired recordings in slices, about how the three classes connect to one another. One weakness of the paper is that the authors make arbitrary and not well-motivated assumptions about the network geometry, and they do not use the flexibility of their simulations to study how their results depend on their network assumptions. A second weakness is that they ignore many known experimental details such as projections into HVC from other nuclei, dendritic computations (the somas and dendrites are treated by the authors as point-like isopotential objects), the role of neuromodulators, and known heterogeneity of the interneurons. These weaknesses make it difficult for readers to know the relevance of the simulations for experiments and for advancing theoretical understanding.*
>
> *Strengths:*
>
> *The authors use conductance-based Hodgkin-Huxley-like equations to simulate spiking activity in a network of neurons intended to model more accurately songbird nucleus*

> *HVC of adult male zebra finches. Spiking models are much closer to experiments than models based on firing rates or on 2-state neurons.*
>
> *The authors include information deduced from modeling experimental current-clamp data such as the types and properties of conductances. They also take into account how neurons in one class connect to neurons in other classes via excitatory or inhibitory synapses, based on sparse paired recordings in slices by other researchers.*
>
> *The authors obtain some new results of modest interest such as how changes in the maximum conductances of four key channels (e.g., A-type K^+ currents or Ca-dependent K^+ currents) influence the structure and propagation of bursts, while simultaneously being able to mimic accurately current-clamp voltage measurements.*
>
> *Weaknesses:*
>
> *One weakness of this paper is the lack of a clearly stated, interesting, and relevant scientific question to try to answer. In the introduction, the authors do not discuss adequately which questions recent experimental and theoretical work have failed to explain adequately, concerning HVC neural dynamics and its role in producing vocalizations. The authors do not discuss adequately why they chose the approach of their paper and how their results address some of these questions.*
>
> *For example, the authors need to explain in more detail how their calculations relate to the works of Daou et al, J. Neurophys. 2013 (which already fitted spiking models to neuronal data and identified certain conductances), to Jin et al J. Comput. Neurosci. 2007 (which already discussed how to get bursts using some experimental details), and to the rather similar paper by E. Armstrong and H. Abarbanel, J. Neurophys 2016, which already postulated and studied sequences of microcircuits in HVC. This last paper is not even cited by the authors.*

We thank the reviewer for this valuable comment, and we agree that we did not clarify enough throughout the paper the utility of our model or how it advanced our understanding of the HVC dynamics and circuitry. To that end, we will revise several places of the manuscript and make sure to cite and highlight the relevance and relatedness of the mentioned papers.

In short, and as mentioned to Reviewer 1, while several models of how sequence is generated within HVC have been proposed (Cannon et al., 2015; Drew & Abbott, 2003; Egger et al., 2020; Elmaleh et al., 2021; Galvis et al., 2018; Gibb et al., 2009a, 2009b; Hamaguchi et al., 2016; Jin, 2009; Long & Fee, 2008; Markowitz et al., 2015; Jin et al., 2007), all the models proposed either rely on intrinsic HVC circuitry to propagate sequential activity, rely on extrinsic feedback to advance the sequence or rely on both. These models do not capture the complex details of spike morphology, do not include the right ionic currents, do not incorporate all classes of HVC neurons, or do not generate realistic firing patterns as seen *in vivo*. Our model is the first biophysically realistic model that incorporates all classes of HVC neurons and their intrinsic properties.

No existing hypothesis had been challenged with our model, rather; our model is a distillation of the various models that's been proposed for the HVC network. We go over this in detail in the Discussion. We believe that the network model we developed provide a step forward in describing the biophysics of HVC circuitry, and may throw a new light on certain dynamics in the mammalian brain, particularly the motor cortex and the hippocampus regions where precisely-timed sequential activity is crucial. We suggest that temporally-precise sequential activity may be a manifestation of neural networks comprised of chain of microcircuits, each containing pools of excitatory and inhibitory neurons, with local interplay among neurons of the same microcircuit and global interplays across the various microcircuits, and with

structured inhibition as well as intrinsic properties synchronizing the neuronal pools and stabilizing timing within a firing sequence.

> *The authors' main achievement is to show that simulations of a certain simplified and idealized network of spiking neurons, which includes some experimental details but ignores many others, match some experimental results like current-clamp-derived voltage time series for the three classes of HVC neurons (although this was already reported in earlier work by Daou and collaborators in 2013), and simultaneously the robust propagation of bursts with properties similar to those observed in experiments. The authors also present results about how certain neuronal details and burst propagation change when certain key maximum conductances are varied.*
>
> *However, these are weak conclusions for two reasons. First, the authors did not do enough calculations to allow the reader to understand how many parameters were needed to obtain these fits and whether simpler circuits, say with fewer parameters and simpler network topology, could do just as well. Second, many previous researchers have demonstrated robust burst propagation in a variety of feed-forward models. So what is new and important about the authors' results compared to the previous computational papers?*

A major novelty of our work is the incorporation of experimental data with detailed network models. While earlier works have established robust burst propagation, our model uses realistic ion channel kinetics and feedback inhibition not only to reproduce experimental neural activity patterns but also to suggest prospective mechanisms for song sequence production in the most biophysical way possible. This aspect that distinguishes our work from other feed-forward models. We go over this in detail in the Discussion. However, the reviewer is right regarding the details of the calculations conducted for the fits, we will make sure to highlight this in the Methods and throughout the manuscript with more details.

We believe that the network model we developed provide a step forward in describing the biophysics of HVC circuitry, and may throw a new light on certain dynamics in the mammalian brain, particularly the motor cortex and the hippocampus regions where precisely-timed sequential activity is crucial. We suggest that temporally-precise sequential activity may be a manifestation of neural networks comprised of chain of microcircuits, each containing pools of excitatory and inhibitory neurons, with local interplay among neurons of the same microcircuit and global interplays across the various microcircuits, and with structured inhibition as well as intrinsic properties synchronizing the neuronal pools and stabilizing timing within a firing sequence.

> *Also missing is a discussion, or at least an acknowledgment, of the fact that not all of the fine experimental details of undershoots, latencies, spike structure, spike accommodation, etc may be relevant for understanding vocalization. While it is nice to know that some models can match these experimental details and produce realistic bursts, that does not mean that all of these details are relevant for the function of producing precise vocalizations. Scientific insights in biology often require exploring which of the many observed details can be ignored and especially identifying the few that are essential for answering some questions. As one example, if HVC-X neurons are completely removed from the authors' model, does one still get robust and reasonable burst propagation of HVC-RA neurons? While part of the nucleus HVC acts as a premotor circuit that drives the nucleus RA, part of HVC is also related to learning. It is not clear that HVC-X neurons, which carry out some unknown calculation and transmit information to area X in a learning pathway, are relevant for burst production and propagation of HVC_{RA} neurons, and so relevant for vocalization. Simulations provide a convenient and direct way to explore questions of this kind.*

> *One key question to answer is whether the bursting of HVC-RA projection neurons is based on a mechanism local to HVC or is some combination of external driving (say from auditory nuclei) and local circuitry. The authors do not contribute to answering this question because they ignore external driving and assume that the mechanism is some kind of intrinsic feed-forward circuit, which they put in by hand in a rather arbitrary and poorly justified way, by assuming the existence of small microcircuits consisting of a few HVC-RA, HVC-X, and HVC-I neurons that somehow correspond to "sub-syllabic segments". To my knowledge, experiments do not suggest the existence of such microcircuits nor does theory suggest the need for such microcircuits.*

Recent results showed a tight correlation between the intrinsic properties of neurons and features of song (Daou and Margoliash 2020, Medina and Margoliash 2024), where adult birds that exhibit similar songs tend to have similar intrinsic properties. While this is relevant, we acknowledge that not all details may be necessary for every aspect of vocalization, and future models could simplify concentrate on core dynamics and exclude certain features while still providing insights into the primary mechanisms.

The question of whether HVC_X neurons are relevant for burst propagation given that our model includes these neurons as part of the network for completeness, the reviewer is correct, the propagation of sequential activity in this model is primarily carried by HVC_{RA} neurons in a feed-forward manner, but only if there is no perturbation to the HVC network. For example, we have shown how altering the intrinsic properties of HVC_X neurons or for interneurons disrupts sequence propagation. In other words, while HVC neurons are the key forces to carry the chain forward, the interplay between excitation and inhibition in our network as well as the intrinsic parameters for all classes of HVC neurons are equally important forces in carrying the chain of activity forward. Thus, the stability of activity propagation necessary for song production depend on a finely balanced network of HVC neurons, with all classes contributing to the overall dynamics.

We agree with the reviewer however that a potential drawback of our model is that its sole focus is on local excitatory connectivity within the HVC (Kornfeld et al., 2017; Long et al., 2010), while HVC neurons receive afferent excitatory connections (Akutagawa & Konishi, 2010; Nottebohm et al., 1982) that plays significant roles in their local dynamics. For example, the excitatory inputs that HVC neurons receive from Uvaeformis may be crucial in initiating (Andalman et al., 2011; Danish et al., 2017; Galvis et al., 2018) or sustaining (Hamaguchi et al., 2016) the sequential activity. While we acknowledge this limitation, our main contribution in this work is the biophysical insights onto how the patterning activity in HVC is largely shaped by the intrinsic properties of the individual neurons as well as the synaptic properties where excitation and inhibition play a major role in enabling neurons to generate their characteristic bursts during singing. This is true and holds irrespective of whether an external drive is injected onto the microcircuits or not. We will however elaborate on and investigate this more during the next submission.

> *Another weakness of this paper is an unsatisfactory discussion of how the model was obtained, validated, and simulated. The authors should state as clearly as possible, in one location such as an appendix, what is the total number of independent parameters for the entire network and how parameter values were deduced from data or assigned by hand. With enough parameters and variables, many details can be fit arbitrarily accurately so researchers have to be careful to avoid overfitting. If parameter values were obtained by fitting to data, the authors should state clearly what the fitting algorithm was (some iterative nonlinear method, whose results can depend on the initial choice of parameters), what the error function used for fitting (sum of least squares?) was, and what data were used for the fitting.*

> *The authors should also state clearly the dynamical state of the network, the vector of quantities that evolve over time. (What is the dimension of that vector, which is also the number of ordinary differential equations that have to be integrated?) The authors do not mention what initial state was used to start the numerical integrations, whether transient dynamics were observed and what were their properties, or how the results depended on the choice of the initial state. The authors do not discuss how they determined that their model was programmed correctly (it is difficult to avoid typing errors when writing several pages or more of a code in any language) or how they determined the accuracy of the numerical integration method beyond fitting to experimental data, say by varying the time step size over some range or by comparing two different integration algorithms.*

We thank the reviewer again. The fitting process in our model occurred only at the first stage where the synaptic parameters were fit to the Mooney and Prather as well as the Kosche results. There was no data shared and we merely looked at the figures in those papers and checked the amplitude of the elicited currents, the magnitudes of DC-evoked excitations etc, and we replicated that in our model. While this is suboptimal, it was better for us to start with it rather than simply using equations for synaptic currents from the literature for other types of neurons (that are not even HVC's or in the songbird) and integrate them into our network model. However, we will certainly highlight the details of this fitting process in the new submission. We will also highlight more technical details in the Methods regarding the exact number of ODEs, the initial conditions to run them, etc.

> *Also disappointing is that the authors do not make any predictions to test, except rather weak ones such as that varying a maximum conductance sufficiently (which might be possible by using dynamic clamps) might cause burst propagation to stop or change its properties. Based on their results, the authors do not make suggestions for further experiments or calculations, but they should.*

We agree that making experimental testable predictions is crucial for the advancement of the model. Our predictions include testing whether eradication of a class of neurons such as HVC_X neurons disrupts activity propagation which can be done through targeted neuron elimination. This also can be done through preventing rebound bursting in HVC_X by pharmacologically blocking the I_h channels. Others include down regulation of certain ion channels (pharmacologically done through ion blockers) and testing which current is fundamental for song production (and there a plenty of test based our results, like the SK current, the T-type Ca^{++} current, the A-type K^+ current, etc). We will incorporate these into the revised manuscript to better demonstrate the model's applicability and to guide future research directions.

https://doi.org/10.7554/eLife.105526.1.sa3